Chapter 1
Optical Studies of Photoexcitations in Polymer/Fullerene Blends for Organic Photovoltaic Applications

C.-X. Sheng and Z.V. Vardeny

Abstract We used a variety of optical probe techniques including broadband femtosecond transient and continuous wave (cw) photomodulation spectroscopies and electroabsorption for studying the photophysics in two typical π-conjugated polymers, namely regio-regular poly (3-hexyl thiophene) (RR-P3HT) with self-organized π-stacked two-dimensional lamellae, and 2-methoxy-5-(2′-ethylhexyloxy) poly(p-para-phenylene-vinylene) (MEH-PPV) with amorphous nanomorphology; both polymers in pristine and blend with fullerene molecules. In the pristine forms we identified singlet excitons as the primary photoexcitations, having typical photoinduced absorption (PA) band that is correlated with stimulated emission. In contrast, in polymer/fullerene blends the photogenerated excitons quickly decay giving rise to a novel photoexcitation species, and the stimulated emission is absent. For the blends we provide strong evidence for the existence of charge transfer complex (CTC) manifold that is formed inside the optical gap of the polymer and fullerene constituents, which is clearly revealed in the electro-absorption spectrum. Because the lowest energy CTC lies below the optical gap then it is possible to directly generate polarons in the blends without involving intrachain excitons in the polymer phase, when using below gap pump excitation. When using excellent quality materials we present evidence that the CTC states are populated in RR-P3HT/fullerene blend within 20 ps following exciton photogeneration in the polymer chains; but no charge polarons are generated on their expense up to ~ 2 ns. Interestingly the CTC states are photogenerated much faster in D-A blends having smaller domain size such as in regio-random P3HT/PCBM and MEH-PPV/C_{60}; however the CTCs do not easily dissociate in these blends because of the large binding energy. Our findings indicate that the CTC state and film morphology play a

C.-X. Sheng · Z.V. Vardeny (✉)
Department of Physics and Astronomy, University of Utah, Salt Lake City, Utah 84112, USA
e-mail: val@physics.utah.edu

C.-X. Sheng
e-mail: cxsheng@njust.edu.cn

C.-X. Sheng
School of Electronic and Optical Engineering, Nanjing University of Science and Technology, Nanjing 210094, Jiangsu, China

Y. Yang and G. Li (eds.), *Progress in High-Efficient Solution Process Organic Photovoltaic Devices*, Topics in Applied Physics 130,
DOI 10.1007/978-3-662-45509-8_1

crucial role in carrier photogeneration in donor-acceptor blends. More thorough investigation of the CTC and its interaction with free polaron excitations may improve the power conversion efficiency of organic solar cells and drive the development of novel photoactive materials.

1.1 Introduction

In recent years, π-conjugated polymer (PCP) based organic solar cells have attracted widespread interest in academia, research institutes and commercial companies. PCPs are promising electronic materials because of their electronic properties, versatility, flexibility, easy of processing and low cost. These factors contribute to the promise that organic solar cells may be able to provide a cost effective alternative compared to inorganic solar cells. In fact the most efficient organic photovoltaic (OPV) cells to date are based on bulk heterojunctions (BHJ) comprised of a blend of a PCP and fullerene, having certified power conversion efficiency (PCE) up to 9 % [1–3]. Despite these significant advances in device performance, the intricacies of charge carrier photogeneration and evolution in donor–acceptor (D-A) blends for OPV applications are still the focus of fundamental research aiming to develop novel photoactive materials and improve the power conversion efficiency of organic solar cell devices [4, 5].

The PCP backbone chain geometry is comprised of series of overlapping σ orbitals formed via sp^2 hybridization where the π-electron is left unbonded, thereby creating a conjugated chain of delocalized π-electrons. These organic semiconductors have a highly anisotropic quasi-one-dimensional (1D) electronic structure that is fundamentally different from the structures of conventional inorganic semiconductors. As a result, the primary photoexcitations in PCPs are bound electron-hole pairs (excitons) with large binding energy, E_B, rather than free charge carriers or excitons with small E_B as in inorganic semiconductors [6]. E_B of singlet intrachain excitons has been experimentally shown to be of order of 0.5 eV [7–9], which is much higher than the room temperature energy, k_BT (where k_B is the Boltzmann factor and T is the temperature), and the most strongly coupled vibration energy of ∼0.2 eV [10–12]. Therefore achieving efficient charge photogeneration by excitons dissociation is the most crucial process in polymer-based solar cells.

The observation of ultrafast photoinduced charge transfer from a conjugated polymer molecule to a C_{60} opened up the potential of PCP based solar cells [13, 14]. This was achieved when the acceptor fullerene molecule was very close to the polymer donor. In more modern D-A blends the donors and acceptors form separate nanosize domains, and are therefore not in close proximity to each other. This poses a problem in OPV devices based on blends if the exciton diffusion length (∼10 nm) is short and thus limits the active layer thickness [15–18]. The donor-acceptor interfacial area available for exciton dissociation is substantially enhanced in PCP/fullerene blend films. However efficient exciton ionization at the D-A interface

cannot by itself guarantee efficient photocurrent generation, because charge transport in the blend needs be efficient. Optimal phase separation of polymer and fullerene domains for balancing the exciton dissociation and charge transport are essential for enhancing solar cell PCE. In order to achieve this goal the bicontinuous interpenetrating network of the electron donor (polymer) and acceptor materials (fullerene) in BHJ structure is an ideal morphology [19].

Although there are still many unanswered questions [20–23], the process of charge photogeneration in polymer/fullerene blend is usually described in a series of sequential steps as follows [4, 5, 24, 25]: (i) Absorption of an above-gap photon in the polymer domains generates intrachain exciton on the polymer chains; (ii) The exciton subsequently diffuses to the polymer/fullerene interface; (iii) where it may be quenched by electron transfer from the polymer to the fullerene. However the significant Coulomb attraction and/or wavefunction overlap between the electron-polaron in the fullerene domain and hole-polaron on the polymer domain results in the formation of charge transfer (CT) exciton state. Then (iv) free charge carrier generation requires further dissociation of these initially generated CT excitons. Importantly the CT exciton can be directly generated using below gap photoexcitation, without involving the first process of intrachain exciton generation [26, 27]. Surprisingly, in this case too the CT exciton may still dissociate into polarons in the polymer and fullerene domains. However these polarons are trapped at the interfaces with relatively long lifetime and do not substantially contribute to the photocurrent density in photovoltaic applications. It is therefore clear that the properties and dynamics of photoexcitations in PCPs and PCP/fullerene blends are of fundamental importance because they play an essential role in the device operation.

In this chapter we review our research studies of photoexcitations in blends of fullerene with two typical PCPs, namely, 2-methoxy-5-(2′-ethylhexyloxy) poly (phenylene-vinylene) (MEH-PPV) and regio-regular poly (3-hexylthiophene) (RR-P3HT), in a broad time interval from femtoseconds to milliseconds and spectral range from 0.1 to 3.5 eV [28–30]. The main experimental technique that we have used is transient photomodulation (PM), which gives information complementary to that obtained by transient photoluminescence (PL), which is limited to radiative processes, or transient photoconductivity (PC), which is sensitive to high mobility photocarriers. The PM method, in contrast, is sensitive to non-equilibrium excitations in *all* states.

1.1.1 Optical Properties of Photoexcitations in Pristine π-Conjugated Polymers and in Polymers/Fullerene Blends

One way to detect and characterize short-lived and long-lived photoexcitations in PCP and PCP/fullerene blends is to study their optical absorption using the PM technique. The photoexcitations in π-conjugated polymers give rise to gap states in the electron and phonon level spectra, respectively. The scheme of the PM experiments is the following: the polymer sample is photoexcited with a ‘pump’

beam of light, and the related change in the optical absorption of the sample is probed in a broad spectral range from the IR to visible spectral range using a variety of 'probe' light sources. The PM spectrum is essentially a difference spectrum, i.e., the difference in the optical absorption ($\Delta\alpha$) spectrum of the polymer when it contains a nonequilibrium photoexcitations concentration and that in the equilibrium ground state. Therefore the optical transitions of the various photoexcitations are of fundamental importance here. In addition, since the PM method does not change the π-electron density in the organic semiconductors, then the π-electron density is constant. Therefore there is a sum rule for $\Delta\alpha$ in the PM spectrum. Namely, there is equal 'amount' of spectral contribution with $\Delta\alpha > 0$ (photoinduced absorption-PA) and $\Delta\alpha < 0$ (photobleaching-PB) [31].

In a strictly 1D chain model, a single charge carrier added onto the polymer chain forms a spin ½ polaron [32]. However, rather than discussing the various electronic states in PCPs in terms of one-electron continuous bands (that is valence and conducting bands), the use of HOMO (highest occupied molecular orbital) and LUMO (lowest unoccupied molecular orbital) has been the preferred description. In the semiconductor description HOMO is the top of the valance band, LUMO is the bottom of the conduction band and this forms a band gap, E_g = LUMO–HOMO [33]. Once the electron-hole interaction is dominant in the model Hamiltonian that describes the electronic states in PCPs, then the excited states become an exciton which is a bound state of electron and hole [34, 35].

Most PCPs belong to the C_{2h} point group symmetry [36]. The notations of odd and even wavefunctions are therefore described in terms of the C_{2h} group irreducible representations with alternating odd (B_u) and even (A_g) parity symmetry [37, 38]. In the exciton description the ground state is $1A_g$ and the first dipole coupled state is the $1B_u$ exciton. In this case the optical gap $E_{op} = E(1B_u) - E(1A_g)$, which is smaller than the free carrier gap, E_g. In case that $E(1B_u) < E(2A_g)$, we still refer to the optical gap $E_{op} = E(1B_u) - E(1A_g)$. We note that among the various photoexcitations the subscript 'g' stands for even (gerade) parity and 'u' stands for odd (ungerade) parity. These symbols are important for possible optical transitions, since one-photon allowed transitions occur between states of *opposite* parity representations, such as $g \rightarrow u$ or $u \rightarrow g$.

In the following section we discuss and summarize the states in the gap and the associated electronic transitions of various photoexcitations in PCPs, and their blend with fullerene; the IR-active vibrations (IRAV's) related to the charged excitations are also briefly summarized here.

1.1.1.1 Optical Transitions of Photoexcitations in Pristine Polymers

It is generally accepted that the $1B_u$ exciton is the primary intrachain photoexcitation when the excitation photon energy is close to the absorption onset of the polymer. However various *interchain* photoexcitations appear to be important in thin films of many PCPs, because of the interchain interaction. The branching of

intrachain and interchain photoexcitations occurs instantaneously in many systems [39, 40]. This topic has been the focus of interest for more than two decades [41]. Here we discuss some intrachain and interchain excitations that are neutral and charged.

Singlet Excitons

The intrachain exciton that is immediately photogenerated upon photon absorption is a neutral, spinless excitation of the polymer chain. In principle optical excitation into higher excited states of the polymer is followed by sub-picosecond nonradiative hot exciton relaxation to the lowest excited state, in which vibrational energy is released [42]. The hot energy relaxation process is due to either vibrational cooling within vibronic sidebands of the same electronic state, or phonon-assisted transitions between two different electronic states, which is termed 'internal conversion' in molecular spectroscopy [43]. Usually internal conversion is the fastest relaxation channel that provides efficient nonradiative transfer from a higher excited state into the lowest excited state of the same spin multiplicity [44, 45]. Before the exciton cools down to the lowest excited state, there are two other ultrafast relaxation processes which may interfere and successfully compete with the internal conversion process. These processes include singlet exciton fission and exciton dissociation [45]. The former process creates two triplet excitons with opposite spins from one singlet exciton, in time faster than the usual intersystem crossing time from the singlet to the triplet manifold [46, 47]; whereas the latter process directly generates charge carriers on two adjacent chains [48, 49]. However in PCPs these two processes happen with much smaller probability than the internal conversion process, and although important for applications, they are not included in our present discussion.

In Fig. 1.1a we summarize the optical transitions of the singlet exciton. Two essential exciton levels ($1B_u$ and mA_g) are shown to play an important role in the exciton picture of PCPs. The mA_g level is known to have strong dipole moment coupling to $1B_u$ as deduced form various optical nonlinear spectra of PCPs analyzed via summation over states model where the "four essential states" are used [37, 38]. We therefore expect two strong optical transitions to form following the $1B_u$ photogeneration, PA_1 from $1B_u$ to mA_g and PA_2 from $1B_u$ to another A_g state, dubbed kA_g.

Following exciton cooling after the lowest exciton state is reached there are still other available processes: The 'cold' exciton may recombine radiatively by emitting light in the form of fluorescence (FL). It may also recombine non-radiatively through recombination centers by emitting phonons. Excitons may be also trapped or undergo an intersystem crossing into the triplet manifold, creating long-lived triplet (T) states. Finally, a singlet exciton may also disassociate into polaron pair (PP) or excimer onto two neighboring chains, which is a process analog to exciton dissociation in polymer/fullerene blends.

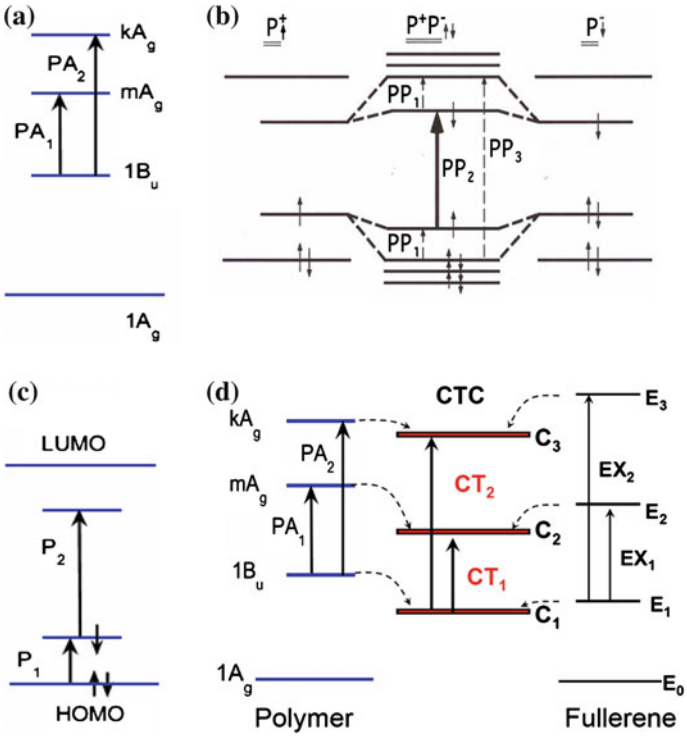

Fig. 1.1 Energy levels and associated optical transitions of exciton (**a**), polaron pair (**b**), positive polaron (**c**) and charge transfer complex (CTC) state (**d**), **a**, **c** is adapted from Sheng et al. [30]. **b** is adapted from Vardeny and Wei [31]

Polaron Pairs

It is now generally recognized that interchain interactions play a strong role in the photophysics of PCP thin films and especially in optoelectronic devices [50–65]. Since the original demonstration of interchain species in films of MEH-PPV by Rothberg et al. [50, 66], a variety of complex optical phenomena in many other PCPs have been ascribed to interchain interactions. Among the complexity of interchain photoexcitation species, a polaron pair (*PP*) [66, 67] may be the simplest and also the most important one. A polaron pair is a bound pair of two oppositely charged polarons, P^+ and P^- formed on two adjacent chains. The strong wave-function overlap leads to large splitting of the P^+ and P^- levels as shown in Fig. 1.1b. For a loosely bound *PP* its dipole allowed transitions are similar to those of the polaron, which will be introduced in the next section. However for a tightly bound *PP* excitations we expect a single transition, PP_2 to dominate the spectrum, as PP_1 is considered to be intraband transition with traditional low intensity, and PP_3 is close to the fundamental transition and therefore difficult to observe (see Fig. 1.1b). In this case there are mainly two states in the gap, and the excitation

species is also known as a neutral *BP* (BP^0) or a 'polaronic exciton'. We note, however that the PP_2 transition is close in spirit to transition PA_2 discussed above for excitons, as a second electron is also promoted to the excited level in the case of *PP*. Then from the experimental point of view, it is not easy to identify and separate the transitions of a trapped exciton from those of a tightly bound *PP* in the PM spectra. They may differ, however in their PA-detected magnetic resonance (PADMR) spectra [68].

Recently, our joint theory-experiment work provided new insight of the photophysics in pristine PCP films. We reported pressure-dependent transient picosecond and continuous-wave photomodulation studies of disordered and ordered films of MEH-PPV. Photoinduced absorption (PA) bands of intrachain excitons and polarons in the disordered film exhibited weak pressure dependence. In contrast, the ordered film exhibited two additional transient PA bands in the mid infrared that dramatically blue-shifted with pressure. Based on high-order configuration interaction calculations, we ascribed the PA bands in the ordered film to excimers [41]. The excimer is a quantum-mechanical superposition of the delocalized neutral exciton and the ionic polaron pair that is obtained in the presence of significant interchain electron hopping.

1.1.1.2 Optical Transitions of Neural and Charged Photoexcitations in Polymer/Fullerene Blends

Charged Photoexcitations: Polarons and Delocalized Polarons

In disordered polymer films a single charge carrier added onto the polymer chain forms a spin-1/2 polaron that results in two states in the gap. Figure 1.1c shows the associated optical transitions for a positively charged polaron, P^+. The polaron energy level in the gap are separated by and energy $2\omega_0$ (P) [69]. Then three optical transitions P_1, P_2 and P_3 are possible [32, 69, 70]. In both oligomers and polymers, however transition P_3 is extremely weak because of the symmetry selection rules; therefore the existence of two optical transitions upon doping or photogeneration indicates that polarons are created [70, 71]. However there might be a disorder-induced relaxation of the above-mentioned optical selection rules that may cause ambiguity as to the number of optical transitions associated with polarons in "real" polymer films, especially for photon energies $\hbar\omega > E_g$.

For highly ordered PCP such as RR-P3HT film, self-organization of the polymer chains results in formation of lamellae structure perpendicular to the film substrate; such 2D lamellae sheets have strong interchain interaction due to the short interlayer distance of the order of 3.8 Å [72]. An interaction model introduced before [73, 74] shows that the interchain interaction in RR-P3HT lamellae splits the intrachain localized polaron levels so that the delocalized polaron (DP) levels are shallower; this results in energy shift of the allowed optically transitions. We note that the transition

DP_1 is red shifted respect to P_1, whereas DP_2 is blue shifted respect to P_2. Moreover, the sum rule: $E(DP_1) + E(DP_2) = E(P_1) + E(P_2)$ approximately holds [73, 74].

Neural Photoexcitations: Charge Transfer Excitons

The charge transfer (CT) exciton or charge transfer complex (CTC) is intermediate excited state between singlet exciton and photogenerated free charge. Evidence for the existence of CTC at the interfaces between the polymer donor and PCBM acceptor domains, and its role as an intermediate state in the free charge photogeneration have been recently reported [4, 5, 21, 26, 75–86]. Several techniques such as electro-absorption, below-gap pump excitation PM, as well as photoluminescence [26, 81, 86] have been applied to study the CTC in polymer/fullerene blends.

However, the commonly used names for CT complexes are diverse, which include polaron pairs [87], geminate polaron pairs [88], interfacial charge pairs [89], charge transfer excitons [86, 90], and exciplexes [91]. The reason for this widely used nomenclature range is the existence of several different steps between the top extreme cases of excitons and free polarons. Although the full quantum mechanical description for CTC is unknown at the present time, nevertheless we may regard the CTC wave function as a linear combination of intrachain exciton ($1B_u$, mA_g, kA_g) of the polymer chain and neighboring states (E_1, E_2, E_3) of the fullerene molecule [92]. Consequently, as shown in Fig. 1.1d we expect two strong optical transitions to form following CT exciton photogeneration, namely CT_1 from C_1 to C_2, and CT_2 form C_1 to C_3 [80, 92].

1.1.1.3 Photoinduced Infrared Active Vibrational Modes (IRAV)

The neutral polymer chain has a set of Raman active A_g-type vibrations that are strongly coupled to the electronic bands via the e-p coupling [10]. These vibrations have been dubbed '*amplitude modes*' (AM) [93]. The AM model has achieved a spectacular success in explaining the resonant Raman scattering (RRS) dispersion as well as photoinduced and doping induced IRAVs in PCPs [10–12]. Because the Raman frequencies are much smaller than the optical gap, and the corresponding IRAV frequencies are much smaller than the energies of photoinduced and doping induced electronic bands, previous applications of AM model were based on the adiabatic approximation [10–12, 93]. However this approximation fails in the case of ordered PCPs such as RR-P3HT/PCBM blends, since the IR-active lines overlap with the electronic transition in this case [73, 74, 94]. Therefore both vibronic and electronic excitations as well as their quantum interference have to be taken into account.

The conductivity spectrum, $\sigma(\omega)$ in this case consists of two parts [11, 95]; one component is determined by the most strongly coupled phonons in the non-adiabatic limit; the other is related to the system response in the absence of phonons.

Within the charge-density wave approximation the sharp features in σ(ω) are given by the relation [96]:

$$\sigma(\omega) \approx \frac{1 + D_0(\omega)[1 - \alpha_p]}{1 + D_0(\omega)[1 + C - \alpha_p]} \tag{1.1}$$

where C is a constant that presents a smooth electronic response; α_p is defined as polaron-vibrational 'pinning parameter' for the trapped polaron excitation; and $D_0(\omega)$ is the 'bare' phonon propagator. The latter is given [93] by the relation: $D_0(\omega) = \Sigma_n d_{0,n}(\omega)$, and $d_{0,n}(\omega) = \lambda_n/\lambda\{(\omega_n^0)^2/[\omega^2 - (\omega_n^0)^2 - i\delta_n]\}$, where ω_n^0, δ_n and λ_n are the 'bare' phonon frequencies, their natural linewidth (inverse lifetime) and electron-phonon (e-p) coupling constant, respectively; and $\Sigma\lambda_n = \lambda$, which is the total e-p coupling.

The poles of (1.1), which can be found from the relation: $D_0(\omega) = -(1 - \alpha_p + C^{-1})$, give peaks (or IRAV's) in the conductivity (absorption) spectrum. We used the IRAV's, which appear as positive absorption lines to identify the charge state of photoexcitations in the ps PM spectra of less ordered PCPs' films [40, 97]. On the other hand the zeros in (1.1), which can be found by the relation: $D_0(\omega) = -(1 - \alpha_p)^{-1}$, give the indentations (or anti-resonances, ARs) in the conductivity (or absorption) spectrum [74, 96].

1.1.2 Experimental Set-up for Measuring Transient and CW Responses

For measuring the transient photoexcitation response in the femtosecond (*fs*) to nanosecond (*ns*) time domains we have used the *fs* two-color pump-probe correlation technique with linearly polarized light beams. Two laser systems have been traditionally used in our laboratory. A high repetition rate, low power laser for the mid-IR spectral range [30]; and a high power low repetition rate laser system for the near-IR and visible spectral range [7].

1.1.2.1 Low Intensity *Fs* Laser System

For the transient PM spectroscopy in the spectral range between 0.55 and 1.05 eV, we used a 100 fs titanium-sapphire oscillator operating at a repetition rate of about 80 MHz, which pumped an optical parametric oscillator (OPO) (Tsunami, Opal, Spectra-Physics) where both signal and idler beams were respectively used as probe beams [30]. In addition a difference frequency of the signal and idler beams set up based on a nonlinear optical crystal was used to extend the probe spectral range from ~0.15 to ~0.43 eV. The pump beam was extracted either from the fundamental at ≈1.55 eV, or from its second harmonics at 3.1 eV. To increase the signal/

noise ratio, an acousto-optical modulator operating at 40 kHz was used to modulate the pump beam intensity. For measuring the transient response at time, t with ≈150 fs time resolution, the probe pulses were mechanically delayed with respect to the pump pulses using a translation stage; the time $t = 0$ was obtained by a cross-correlation between the pump and probe pulses in a nonlinear optical crystal. Typically the laser pump intensity was kept lower than 5 μJ/cm^2 per pulse, which corresponds to ≈10^{16}/cm^3 initial photoexcitation density per pulse in the polymer films. This low density avoids the complications usually encountered with high power lasers such as bimolecular recombination and stimulated emission; both processes tend to increase the recombination rate of the photoexcited excitons.

The transient PM signal, ΔT/T(t) is the fractional changes ΔT in transmission T, which is negative for photoinduced absorption (PA) and positive for photoinduced bleaching (PB) at photon energy above the absorption onset, and stimulated emission for photon energies below the optical gap when overlap exists with the PL spectrum. The pump and probe beams were carefully adjusted to get complete spatial overlap on the film, which was kept under dynamic vacuum. In addition the pump/probe beam-walk caused by the translation stage was carefully monitored and the transient response was adjusted by the beam walk measured response.

Since some photoexcitations may live longer than the time interval between successive pulses, then a *background PA* may be formed. An advantage of this mid-IR laser system is that the background PA spectrum can be readily measured using the same pump/probe set up as for the ultrafast response. This was achieved by measuring the PA signal at $t < 0$ since the probe pulse in this situation arrives before the pump pulse, and therefore is affected by the 'left-over' photoexcitations in the film that survive in between successive pulses [98]. Recall that the background PA is modulated at frequency of 40 kHz, and thus is sensitive to long-lived photoexcitations in the film having lifetime longer than $\sim 1/f$ (= 25 μsec).

1.1.2.2 High Intensity *Fs* Laser System

For the near IR and visible range we have used the high intensity laser system [7]. This laser system is based on a Ti:sapphire regenerative amplifier that provides pulses of 100 *fs* duration at photon energies of 1.55 eV, with 400 μJ energy per pulse at a repetition rate of 1 kHz. The second harmonic of the fundamental at 3.1 eV was used as the pump beam. The probe beam was a white light supercontinuum within the spectral range from 1.1 to 2.8 eV, which was generated using a portion of the Ti-sapphire amplifier output in a 1-mm-thick sapphire plate. To improve the signal-to-noise ratio in our measurements, the pump beam was synchronously modulated by a mechanical chopper at exactly half the repetition rate of the Ti:sapphire laser system (≅500 Hz). The probe beam was mechanically delayed with respect to the pump beam using a computerized translation stage in the time interval, t up to 200 *ps*. The beam spot size on the sample was about 1 mm in diameter for the pump beam and about 0.4 mm diameter for the probe beam. The pump beam intensity was set below 300 μJ/cm^2 per pulse, which is below the signal

saturation limit. The wavelength resolution of this system was about 8 nm using a 1/8-meter monochromator having a 1.2 mm exit slit, which was placed in the probe beam after it had passed through the sample. The transient spectrum ΔT/T(t) was obtained using a phase sensitive technique with a resolution in $\Delta T/T \approx 10^{-4}$.

1.1.2.3 CW Optical Measurements

For the cw PM spectroscopy we used a standard PM setup at low temperatures [31] and references therein. The excitation beam was an Ar^+ laser with several lines in the visible spectral range and UV at 353 nm, which was modulated with a mechanical chopper at a frequency of ~300 Hz. The probe beam was extracted from a tungsten lamp in the spectral range 0.25–3 eV. A combination of various diffraction gratings, optical filters, and solid-state detectors (silicon, germanium and indium antimonite) were used to record the PM spectra. The spectral resolution was about 2 nm in the visible spectral range and 4–10 nm in the near infrared range, with ΔT/T resolution of $\approx 10^{-6}$.

In order to retrieve the mean polaron lifetime, τ, the frequency response of both in-phase and quadrature PA components were measured, and were fit to an equation

$$\Delta T(f)/T = G\tau[1 + (i2\pi f\tau)^P] \tag{1.2}$$

where G is the generation rate (proportional to the laser intensity) and p (< 1) is the dispersive parameter that describes the recombination dispersion of polarons due to disorder in the system [99].

In addition, in order to identify photogenerated polarons in the photomodulation spectrum we also measured the doping induced absorption spectrum of the polymers, where a thin polymer film was exposed to low pressure iodine gas for ~10 s. The doping induced absorption spectrum was then obtained by subtracting the optical density of the pristine polymer film from that of the doped film.

1.1.2.4 Electroabsorption

EA has provided a sensitive tool for studying the band structure of inorganic-semiconductors [100] as well as organic- semiconductors [38, 101, 102]. In general the EA spectrum emphasizes optical transitions at singularities of the joint density of states that respond sensitively to an external field, and therefore are lifted from the broad background of the absorption continuum [103]. The EA sensitivity, however diminishes for more confined electronic transitions, because the applied electric fields (of the order of 100 kV/cm) are too small of a perturbation to cause sizable changes in their associated optical transitions. Consequently EA spectroscopy has been an ideal tool to separate exciton bands from the continuum band [103]. For example in 1D semiconductors the confined excitons were shown to exhibit a quadratic Stark effect, where the EA signal scales with F^2, and its

spectrum resemble to a first derivative of the absorption edge. Whereas the EA spectrum related to the continuum band was found to scale with $F^{1/3}$, and showed Franz-Keldysh (FK) type oscillation. One of the most notable examples of the application of EA spectroscopy to organic semiconductors is polydiacetylene, in which EA spectroscopy was able to separate absorption bands of quasi-1D excitons from that of the continuum band [103]. The separation of the EA contribution of excitons and continuum band was then used to obtain the exciton binding energy in polydiacetylene, which was found to be $\sim$0.5 eV [103].

For the EA measurements we used a PCP film spin cast on a substrate with patterned metallic electrodes [104]. The EA substrate consisted of two interdigitated sets of a few hundred 30 μm wide gold electrodes, which were patterned on a sapphire substrate. The sample was placed in a cryostat for low temperature measurements. By applying a potential V to the electrodes a typical electric field, $F \sim 10^5$ V/cm was generated with $V = 300$ V and $f = 1$ kHz parallel to the film. For probing the EA spectrum we used an incandescent light source from a Xe lamp, which was dispersed through a monochromator, focused on the sample, and detected by a UV-enhanced silicon photodiode. We measured ΔT with probe light parallel and perpendicular to the direction of the applied electric field using a lock-in amplifier set to twice the frequency ($2f$) of the applied field [104], and verified that no EA signal was observed at f or $3f$. ΔT and T spectra were measured separately and the polarized EA spectrum was obtained from the ratio $\Delta T/T$. The detailed description for the EA experimental setup was presented in [7].

1.1.2.5 Solar Cell Fabrication and Testing [105]

The bulk heterojunction OPV solar cell devices were composed of a transparent indium tin oxide (ITO) anode; a spin-cast polyethylenedioxythiophene/polystyrene sulphonate (PEDOT/PSS) hole transport layer; an active material layer spin-cast from a blend of P3HT donor and PCBM acceptor; and capped with LiF/Al cathode. The ITO-coated glass substrates (Delta Technology, CB-50IN) were cleaned by ultrasonic treatment and oxygen plasma treatment. The PEDOT/PSS (Clevios, P VP AI 4083) layer was spin-cast at 5,000 RPM for 20 s at ambient conditions, and transferred to a nitrogen-filled glovebox ($O_2 < 1$ ppm) for annealing at 120 °C for 30 min. The organic blend comprised of P3HT (Plextronics, Plexcore OS 2,100) and PCBM (purity > 99.9 %) that were prepared at weight ratio of 1.2:1 in 1,2-dichlorobenzene solution that was heated at 50 °C for 30 min. and stirred overnight. The device active layer was spin-cast from the solution blend at 400 RPM for 6 min and annealed at 150 °C for 30 min; the device active area was 2 mm × 2.5 mm. The fabrication was completed by thermally evaporating a 1 nm thick film of LiF layer followed by a 100 nm thick film of Al. Finally the device was encapsulated under a cover glass using UV-curable optical adhesive (Norland, NOA 61). The device I-V characteristics under illumination were measured using a Keithley 236 Source-Measure unit. The light intensity of the solar simulator composed of a xenon lamp

and an AM 1.5G filter was calibrated at 100 mW/cm^2 using a pre-calibrated silicon photovoltaic cell. The OPV device output current was measured using phase sensitive lock-in technique.

1.2 Photoexcitation Dynamics in Pristine MEH-PPV and MEH-PPV/Fullerene Blends

1.2.1 Transient Photomodulation Spectroscopy of Pristine MEH-PPV Films

MEH-PPV is one of the most studied PCP. Due to its side group the MEH-PPV polymer is able to form an ordered phase when films are cast from 'bad' solvents such as toluene [106, 107]. In such films two or more polymer chains may be coupled together due to increased interchain interaction. Under these conditions the primary photoexcitations may contain interchain components that spread over two (or more) chains. The photoexcitations delocalization over several polymer chains may lead to several characteristic properties, including [104]: (i) reduced PL quantum efficiency; (ii) PL red-shift; (iii) relatively large generation efficiency of polaron pair and excimer excitations; (iv) substantially delayed PL due to polaron pair and excimer recombination; and (v) increased photogeneration efficiency of charge carriers in C_{60} doped polymer films.

Figure 1.2a shows the transient PM spectrum of a MEH-PPV film casted from toluene solution at "t = 0 ps". It contains excitons with PA_1 and PA_2 bands at 0.95 and 1.35 eV, as well as polarons with P_1 and P_2 bands at 0.35 and 1.6 eV, respectively. In addition, there is also a stimulated emission (SE) band as well as a photobleaching band. We showed [30] that the polarons PA bands in the PM spectrum have a slower dynamics compare to that of the exciton PA bands and the associated SE, indicating that they belong to different photoexcited species Fig. 1.2b. The band P_1 and P_2 were identified as due to polarons, since the cw polaron band P_1 also peaks at about the same value, i.e. $h\omega$(probe) = 0.4 eV. However because there are no accompanying IRAVs at room temperature, we concluded that the polarons photogenerated at t = 0 ps are Coulombically bound forming polaron pairs, or may be highly correlated forming excimers. Recently our joint theory-experiment work reported pressure-dependent transient picosecond and continuous-wave photomodulation studies of disordered and ordered films of MEH-PPV. Photoinduced absorption bands of intrachain excitons and polarons in the disordered film exhibited weak pressure dependence [41]. In contrast, the ordered film exhibited two additional transient PA bands in the mid infrared that blue-shift dramatically with pressure. Based on high-order configuration interaction calculations, we ascribed the PA bands in the ordered film to excimers [41].

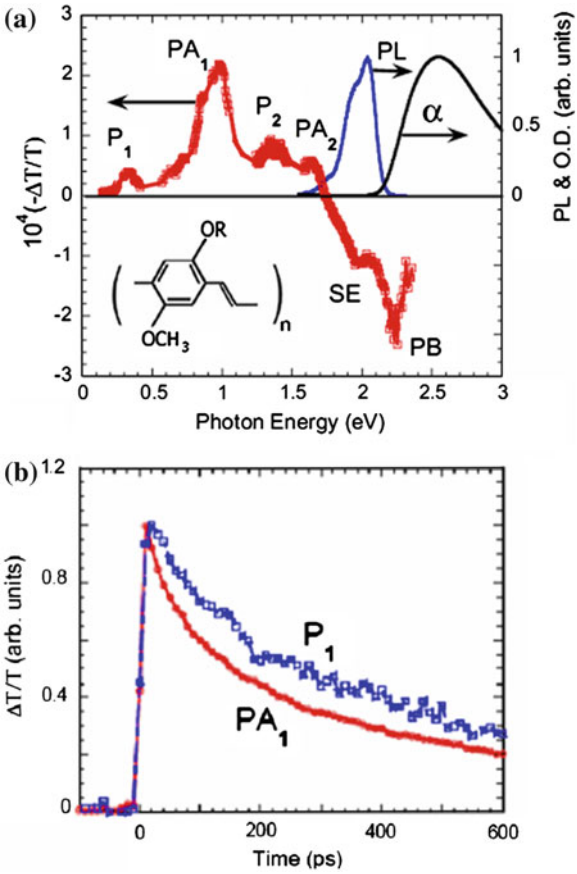

Fig. 1.2 **a** The transient PM spectrum at t = 0 of pristine MEH-PPV film cast from toluene solution in the spectral range of 0.15–2.4 eV; the *inset* shows the polymer backbone structure. Various spectral bands are assigned; P_1 and P_2 are for polarons; PA_1 and PA_2 are for excitons; and SE and PB are stimulated emission and photobleaching of the absorption, respectively. The absorption and photoluminescence spectra are also shown for comparison. **b** The decay dynamics of the exciton and polaron bands (Adapted from Sheng et al. [30])

1.2.2 Photomodulation of MEH-PPV/C_{60} Blends

1.2.2.1 Transient Photomodulation Spectroscopy with Above-Gap and Below-Gap Pump Excitations

It has been known that C_{60} doping of many π-conjugated polymers promotes a strong photoinduced charge transfer process, where the photogenerated excitons dissociate into positive polaron on the polymer chain and negative polaron on the C_{60} molecule [13]. In (1:1 by weight) MEH-PPV/C_{60} blend it was measured that the photoinduced dissociation occurs with time constant of ~50 fs [108].

Figures 1.3a and 1.4 show the transient PM spectra of a 1:1 MEH-PPV/C_{60} blend with above-gap (AG 400 nm) and below-gap (BG 800 nm) excitation, respectively. The $t = 0$ PM spectrum with AG excitation contains three PA bands peaked at 0.4 eV (P_1), 1.5 eV (P_2), and 1.0 eV (PA_1), which are respectively due to polarons and excitons on the polymer chains; and an accompanying PB band above

2.2 eV. The dissociation process of exciton in 50 % C_{60}-doped film occurs within 200 *fs* (Fig. 1.3b inset), in agreement with transient measurements done in other laboratories [109]. The inset to Fig. 1.3a shows that P_1 polaron and PB (at 2.5 eV) increase with time *on the expense* of PA_1 exciton decay; so that at $t \sim 10$ *ps* only the polaron PA bands P_1 and P_2 remain in the PM spectrum, in contrast to pristine MEH-PPV [30]. This shows that with AG excitation the intrachain excitons *separate into polarons* via an electron transfer reaction from the polymer chain (donor) onto the C_{60} molecule (acceptor); and vice versa. This is the traditional photoinduced charge transfer mechanism postulated to occur in the blend [13]. In Fig. 1.3b we show that P_1 band has a much longer lifetime compared with PA_1 of excitons, as well as with P_1 lifetime (Fig. 1.2b) in pristine MEH-PPV.

Figure 1.4 shows that with BG excitation, which is not capable of generating intrachain excitons on the polymer (i.e. PA_1 is not formed in the PM spectrum), *polarons are still photogenerated with estimated quantum efficiency (QE) of* ~ 100 *%*.

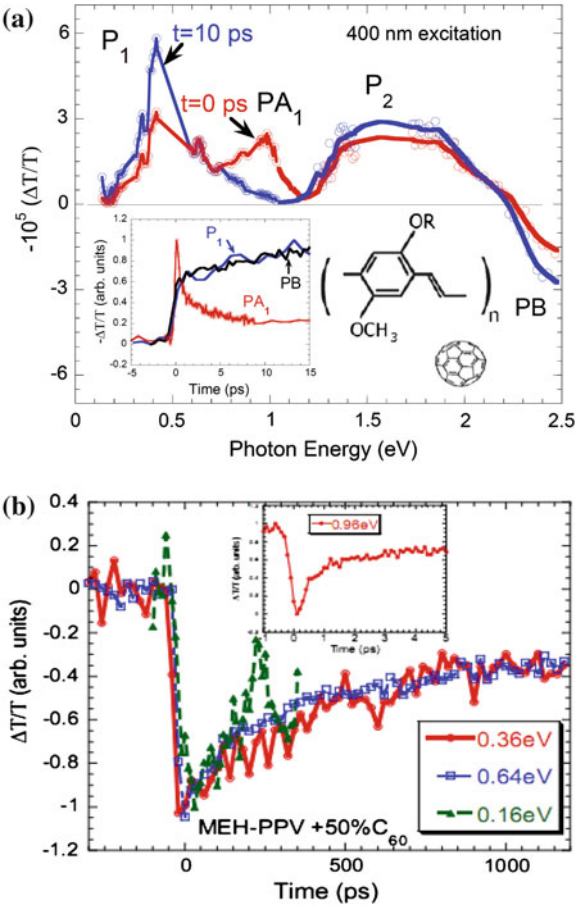

Fig. 1.3 **a** The transient PM spectrum of MEH-PPV/C_{60} (1:1) blend film with above gap at t = 0 (*red*) and 10 ps (*blue*). The polaron PA bands P_1 and P_2, exciton PA_1, and PB band are assigned. The *insets* in **a** show the ultrafast dynamics of the various bands up to 15 ps, and the polymer and fullerene backbone structures, respectively. **b** PA decay dynamics at various probe energies. The *inset* to **b** is the ultrafast PA_1 decay measured at 0.96 eV. **a** is adapted from Drori et al. [26], **b** is adapted from Sheng [110]

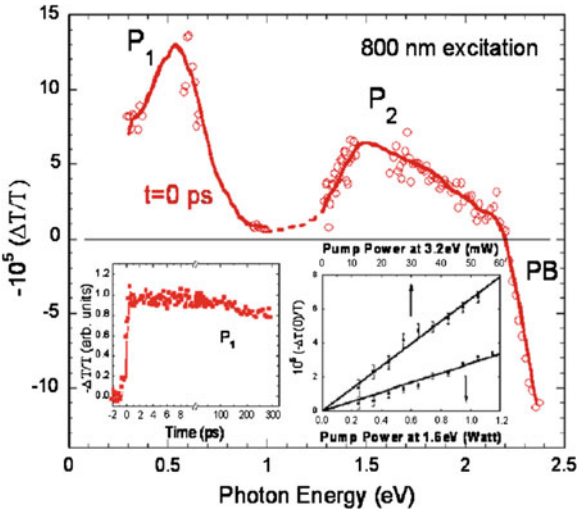

Fig. 1.4 The transient PM spectrum of MEH-PPV/C_{60} (1:1) blend film with below-gap excitation at t = 0. The polaron PA bands P_1 and P_2, exciton PA_1, and PB band are assigned. The *insets* shows the P_1 band dynamics up to 300 ps (*left*) and its excitation intensity dependence with above-gap and below-gap (*right*) (Adapted from Drori et al. [26])

This can be inferred from the two polaron bands P_1 and P_2 in the PM spectrum that are generated instantaneously (Fig. 1.4 inset). The BG excitation polarons are long-lived (Fig. 1.4 inset), and we thus conclude that they remain localized following photo-generation. This indicates that the 1.55 eV pump is a direct transition into a state that is formed below the polymer and fullerene optical gaps, which is capable of creating separated charges on the polymer and fullerene without the need of an intermediate step such as intrachain exciton. This can be readily explained if this state is a CTC lying inside the gap, *below* the donor and acceptor lowest lying excitons [75].

It is interesting to compare our results in optimum blend with blends of MEH-PPV films with less C_{60} molecules. Figure 1.5a shows the mid-IR PM spectra of 10 % C_{60} doped (by weight) MEH-PPV film at various delay times: t = 0, 2 and 100 *ps* following the pulse excitation [110]. It is seen that the PA_1 exciton band at 0.9 eV gradually disappears from the PM spectrum as the exciton dissociation occurs. In parallel with the decrease of PA_1, photoinduced IRAV at $\sim$0.18 eV gradually appears in the PM spectrum (Fig. 1.5b). This shows that photogenerated excitons decay into charge polarons indicating that exciton dissociation indeed occurs between the polymer chains and C_{60} molecules [13, 111]. However, the charge transfer reaction is not as fast as that measured in the (1:1) MEH-PPV/C_{60} blend [108]. From Fig. 1.5b we conclude that the IRAV dynamics is *delayed* respect to the exciton PA_1 instantaneous response. From the IRAV transient here we estimate that the IRAV's are photogenerated within $\sim$2 ps in the 10 % C_{60} doped film, in contrast to the time constant of about 50 fs in 50 % C_{60} doped films

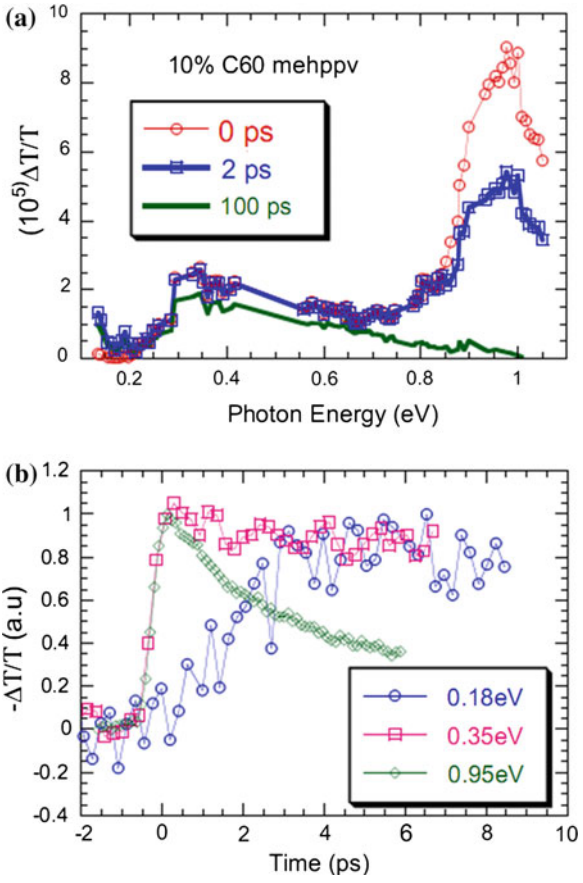

Fig. 1.5 **a** Transient PM spectra of 10 % C_{60} doped MEH-PPV film at t = 0, 2 ps, and 100 ps. **b** Transient PM responses at various probe energies (From Sheng [110] with permission)

[108]. This indicates that the photoinduced charge transfer reaction in C_{60} doped films is actually limited by the *exciton diffusion* towards C_{60} molecules close to the polymer chains. Consequently the exciton wavefunction in MEH-PPV films is not as extended as previously thought. The same conclusion was drawn for C_{60} doped DOO-PPV films, where it was estimated [112] that the exciton diffusion constant to reach the C_{60} molecules in the film is of the order of 10^{-4} cm^2/s.

1.2.2.2 CW Photomodulation Spectroscopy with Above-Gap and Below-Gap Excitations

Figure 1.6a shows that the cw PA spectrum of polarons generated with BG and AG excitation are indistinguishable from each other; both spectra contain the signature of separated polarons, namely IRAVs, and two PA bands P_1 and P_2. We thus conclude that a mechanism exists in the blend through which BG excitation is able

to generate charges on the polymer chains; in agreement with the transient spectrum in Fig. 1.4. However polarons generated with BG excitation are much longer lived (Fig. 1.6a inset), since the P_1 band frequency dependent steeply increases at low f down to $\sim$10 Hz for BG excitation, whereas the P_1 increase at low f saturates at $\sim$100 Hz for AG polarons. In fact by fitting the frequency dependence we found that the polaron lifetime with BG excitation is about *two-orders of magnitude longer* than that of polarons with AG excitation. This cannot be explained simply

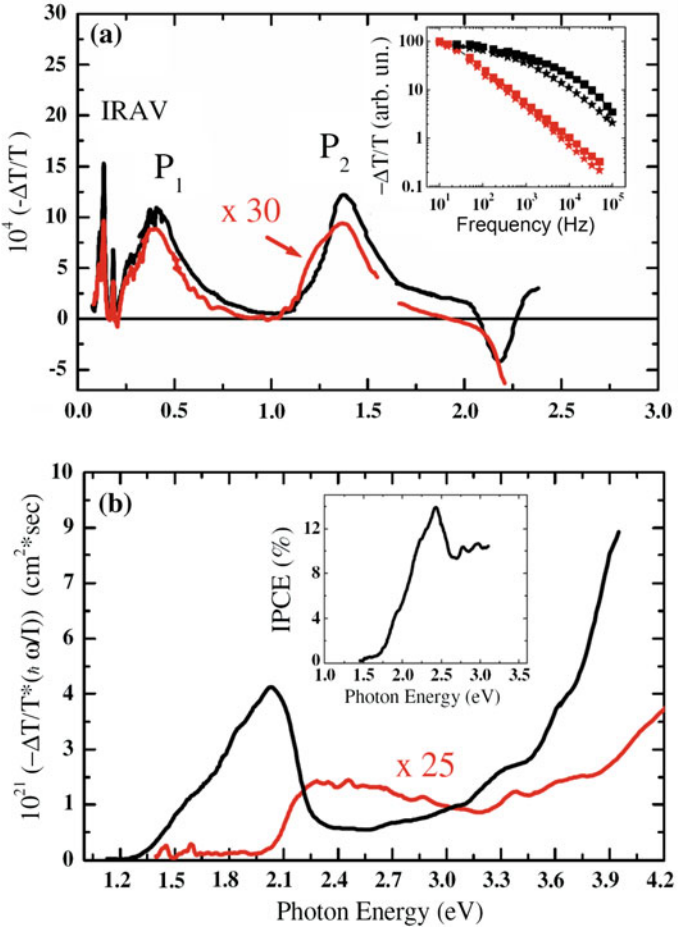

Fig. 1.6 **a** The cw PM spectrum of MEH-PPV/C_{60} (1:1) blend film at 80 K, obtained with above gap (*black*) and below-gap (*red*, X 30) excitation. The polaron PA bands P_1, P_2 and IRAV's are assigned. The *inset* shows the polaron P_1 band modulation frequency response measured with above-gap (*black*) and below-gap (*red*) excitation at two intensities that differ by a factor 5. **b** The P_1 action spectra/impinging photon of the MEH-PPV/C_{60} blend (*black*) and pristine MEH-PPV films (*red*, X 25). The *inset* shows the action spectrum of the short-circuit current in a solar cell based on the MEH-PPV/C_{60} blend (Adapted from Drori et al. [26])

by bimolecular recombination kinetics [113], where the polaron density with BG excitation is much smaller (see the decay kinetics in Fig. 1.6a for various excitation intensities). We thus conclude that polarons with BG excitation are localized, having much slower recombination kinetics.

Figure 1.6b shows the polaron P_1 action spectrum in pristine MEH-PPV and MEH-PPV/C_{60} blend. From the action spectra we conclude that polarons in pristine polymer are generated *exclusively* with AG excitation, having a clear onset at the polymer optical gap ($\sim$2.1 eV). In contrast, polarons in the blend can be photogenerated with BG excitation with high QE down to $\sim$1.3 eV. The *apparent* band in the action spectrum for $\hbar\omega < 2$ eV is caused by the immense increase in the polaron lifetime with BG excitation; and thus for calculating the effective BG polaron QE/absorbed photon, the action spectrum shown in Fig. 1.6b should be reduced by the ratio of BG and AG polaron lifetime (a factor of $\sim$120). Nevertheless the BG absorption also steeply decreases (Fig. 1.7a inset), so that these two effects somewhat compensate each other, giving a *substantial* polaron QE for BG excitation in the blend. The inset to Fig. 1.6b shows the photocurrent (PC) action spectrum in a solar cell device made with the MEH-PPV/C_{60} blend for the active layer. Although it has a BG tail down to $\sim$1.5 eV [114, 115], PC is substantially lower with BG than with AG excitation; in sharp contrast with the P_1 action spectrum shown in Fig. 1.6b. This is compelling evidence that BG excitation results in polarons that are less capable to substantially contribute to the device photovoltaic response, because they are less mobile compared to polarons generated with AG excitation. However the BG polaron generation may be detrimental to the device operation, since these localized polarons may serve as traps and recombination centers to the more mobile photocarriers generated with AG excitation.

1.2.2.3 Electroabsorption Spectroscopy

A direct proof for the existence of a CTC below the gap in the blend is provided by the EA spectroscopy. Figure 1.7a and b summarize the EA spectra of pristine polymer and C_{60}, as well as their blend, respectively. In all cases we found that near the band-edge EA $\sim F^2$, where F is the field strength [7]. This has been explained as due a second order Stark shift of the lowest lying exciton state and its phonon replicas [7]. Indeed Fig. 1.7a shows derivative like feature with zero-crossing at 2.2 eV ($\approx$E($1B_u$)) for MEH-PPV, and 2.4 eV ($\approx$continuum onset) for C_{60}. Figure 1.7b shows that the EA spectrum in the blend for $\hbar\omega$ >2 eV is a superposition of the EA spectra of the constituents, which is somewhat broader due to excess disorder in the blend. However the EA spectrum of the blend also contains a prominent derivative-like feature with zero-crossing at $\sim$1.57 eV, similar in shape as the EA of the $1B_u$ state in the polymer (Fig. 1.7a). We thus conclude that this is due to Stark shift of a *real state* that is formed in the blend below the optical gaps of both constituents. The BG absorption spectrum of the blend (Fig. 1.7a inset) indeed

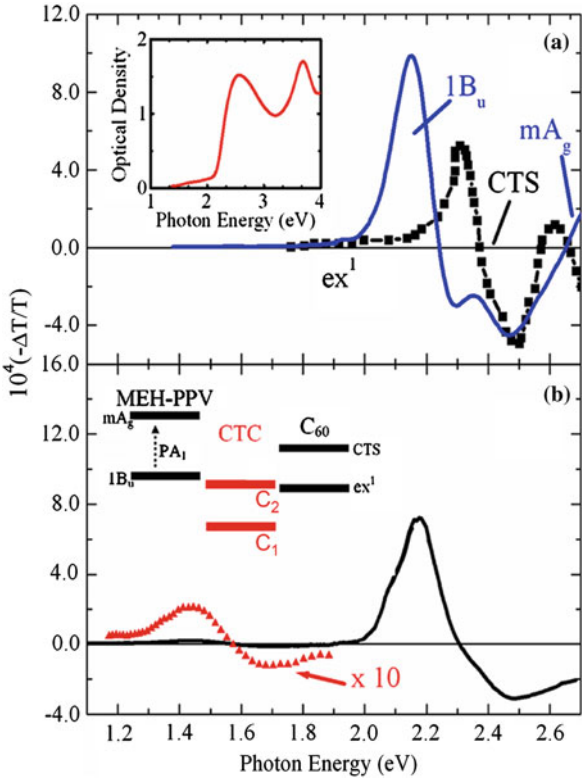

Fig. 1.7 The EA spectra of pristine MEH-PPV (*blue line*) and C_{60} (*black squares*) (**a**); and MEH-PPV/C_{60} blend (**b**), where the below-gap spectrum is also shown multiplied by a factor of 10. The various bands $1B_u$, mA_g for the polymer [113], and CTS for the C_{60} [104] [for their definition see text and *inset* **b**] are assigned. The *inset* in **a** shows the absorption spectrum of the MEH-PPV/C_{60} blend; whereas the *inset* in **b** shows schematically the respective energies of the lowest lying excitons in the MEH-PPV and C_{60}, and those of the CTC formed between the polymer and fullerene (From Drori et al. [26] with permission)

shows a long tail down to ~1.3 eV, that is too weak to produce a substantial contribution to the EA, unless the dipole moment of this BG state is very strong. Traditionally a CTC state has strong dipole moment [104], and thus is a natural candidate to explain the BG state formed in the blend. This is schematically shown in Fig. 1.7b inset, where the CTC at ~1.57 eV lies below the lowest lying singlet excitons in MEH-PPV (~2.1 eV) and C_{60} (~1.85 eV). In fact the CTC state lies even below the respective lowest triplet exciton level of the constituents; and this explains the high QE of polaron generation for this blend [75].

1.2.3 Transient Photomodulation Spectroscopy of Polymer Blends with Strong Acceptor Molecules

One current deficiency in organic solar cells however, is negligible absorption in the near-infrared (NIR) spectral range of the solar spectrum, which lies within the optical gap of most conventional organic blend systems. Several techniques have been developed to increase the near-infrared absorption including using lower-bandgap polymers [116], multiactive layer devices [117, 118], and more recently, charge-transfer complexes [4, 26, 75]. Another viable candidate may be a polymer/acceptor blend with a molecular acceptor having larger electron affinity than the traditional fullerene molecules. Below-gap optical excitation of such organic donor/acceptor blends reveals subtle features attributed to CTC, which have recently attracted much attention by their property of extending optical absorption into the NIR spectral range. One proposal is to use 2,4,7-trinitro-9-fluorenone (TNF) [molecular structure given in Fig. 1.8d inset] as the strong acceptor.

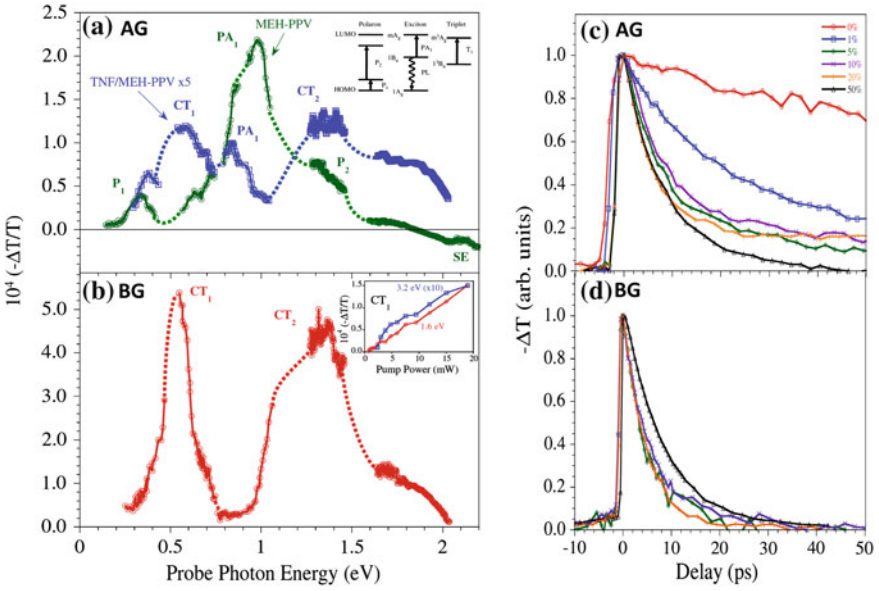

Fig. 1.8 **a** Femtosecond PM spectrum at t = 0 of (1:1) MEH-PPV/TNF pumped at 3.2 eV (*blue squares*) compared to that in pristine MEH-PPV (*green circles*). The PA bands P_1, P_2, CT_1, and CT_2 are denoted. *Inset* shows the energy levels and optical transitions of polarons, singlet excitons, and triplet excitons in MEH-PPV. **b** PM pectrum of (1:1) MEH-PPV/TNF blend pumped at 1.6 eV. *Inset* shows the PA vs pump intensity of (1:1) MEH-PPV/TNF probed at 0.69 eV (CT_1) for both BG and AG excitation. **c** and **d** Femtosecond dynamics vs TNF concentration in various MEH-PPV/TNF blends for the CT_1 PA band probed at 0.67 eV and pumped at 3.2 eV (AG) and 1.55 eV (BG), respectively (Adapted from Holt et al. [80])

When the MEH-PPV as electron donor and TNF acceptor are blended, new nonadditive optical transitions are observed [119, 120]. Bakulin et al. reported that the absorption spectrum of such blends extends into the near-infrared spectral range, along with a nonadditive photoluminescence (PL) band; new and shifted infrared-active vibrational bands and Raman-scattering spectra; and a new photo-induced absorption (PA) band. The polymer PL is strongly quenched, similar as in other polymer/fullerene blend systems [121]. In addition, TNF has a relatively high electron affinity [122] with a lowest unoccupied molecular-orbital (LUMO) energy difference from that of MEH-PPV larger than that of C_{60}; this should prevent electron back transfer after charge separation [123].

Such a body of evidence would nominate TNF as an exceptional candidate for bulk-heterojunction photovoltaic applications. In reality though, actual photocurrent in TNF devices was found to be [124] orders of magnitude lower than that in more conventional polymer/C_{60} blend devices. Yet TNF remains a model prototype for studying the influence of CTC states in organic photovoltaics. Recently a series of significant follow-up works on polymer/TNF blends has been performed [119–121], including the ultrafast dynamics measurements of an MEH-PPV doped with a low concentration of TNF molecules [125].

Figure 1.8a shows the transient PM spectra at t = 0 in a (1:1) blend of MEH-PPV/TNF compared to pristine MEH-PPV film when pumped at 3.1 eV. The transient PM spectrum of the pristine film contains two PA bands. These are P_1 peaking at 0.3 eV due to polaron excitations; and PA_1 due to excitons that peaks at (1 eV). The PA_1 band in the blend is quenched relative to that in the pristine film. The missing stimulated emission in the composite samples is due to the strongly quenched PL of MEH-PPV in the mixture but may also be due to the ground-state absorption tail in the blend. The most conspicuous contribution in the ultrafast PM spectrum of the blend is the peak around 0.5 eV that appears blue-shifted compared to the P_1 peak at 0.3 eV. The new PA band could be better resolved with BG excitation (Fig. 1.5b), where the PA_1 contribution is completely absent. This is consistent with the interpretation that the PA_1 band is due to excitons, which cannot be photogenerated with BG excitation. Together with the new PA band in the mid infrared spectral range (0.5 eV) we also found a new PA band in the near-infrared spectral range ($\sim$1.45 eV; Fig. 1.8a, b. Considering the short lifetime of these PA bands (Fig. 1.8c and d for CT_1 band), it would be consistent to consider that the PA bands at 0.5 eV and at 1.45 eV are completely new bands that are associated with the CTC itself; they are therefore labeled CT_1 and CT_2, respectively. In addition to the novel CT bands, the PA_1 exciton band in the blended system is almost quenched at t = 0 when pumped AG of the polymer. Therefore most photogenerated excitons reach the CTC state before the time resolution of the laser system (150 fs). To ensure that there was no artifact from exciton/exciton annihilation or two photon absorption in our BG experiments, we checked that the transient PA signal is linear versus pump intensity (Fig. 1.8b inset). Indeed, the pump intensities are well below the threshold for such interactions. (10^{19} cm^{-3})

We conclude that the inefficiency of the MEH-PPV/TNF blend for photovoltaic applications was exposed by the fast dynamics obtained for the CT photoexcitations, although the CTC states are formed in record time.

1.3 Photoexcitation Dynamics in Printine RR-P3HT and RR-P3HT/Fullerene Blends

One of the most studied bulk heterojunction (BHJ) organic photovoltaic materials is the blend RR-P3HT (Fig. 1.9a inset) and [6] -phenyl-C_{61}-butyric acid methyl ester (PCBM) (Fig. 1.9b inset), which is often considered as a "model BHJ system" [4, 5, 126]. The P3HT/PCBM blend films are characterized by charge photogeneration with high efficiency, and phase separated fullerene and polymer networks that

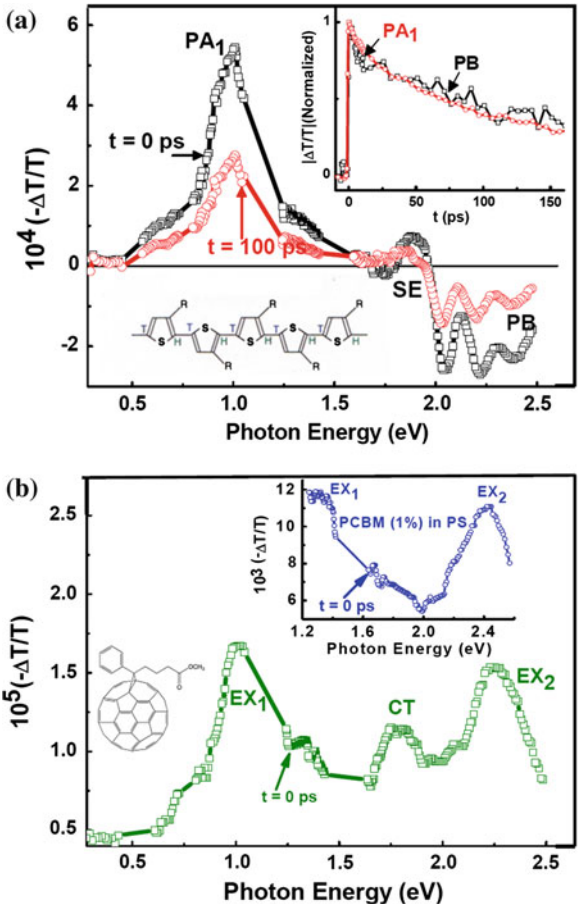

Fig. 1.9 **a** The transient photomodulation spectrum of pristine RR-P3HT film at t = 0 and t = 100 ps, respectively; the exciton bands PA_1, SE and PB are indicated. The *right inset* shows the transient decay of PA_1 and PB bands up to t = 200 ps; the *left inset* shows the polymer backbone chain. **b** The transient photomodulation spectrum of a PCBM film at t = 0; the exciton PA bands EX_1 and EX_2, and CT exciton band are indicated. The *right inset* shows *DT/T*(0) spectrum of isolated PCBM molecules in polystyrene (weight ratio of 1:100) that lacks the CT exciton band. The *left inset* shows the PCBM molecular structure (Adapted from Singh et al. [92])

facilitate charge transport. Consequently high power conversion efficiencies up to ~4.5 % can be obtained in solar cells based on RR-P3HT/PCBM BHJ photovoltaic devices [19, 127]. Numerous steady-state and time-resolved spectroscopic studies have been conducted in pristine P3HT and P3HT/PCBM blend in order to understand the properties and evolution of neutral and charged photoexcitations; but many aspects of the photophysics still remain unclear [20, 21, 30, 39, 60, 73, 74, 86, 128–137]. As a result the process of charge photogeneration in this blend is still a matter of debate. In contrast to the labyrinth photosynthesis process that has evolved in nature [138], the charge photogeneration process in organic photovoltaic cells utilizes one type of heterojunction between two organic semiconductors. The two organic semiconductors, dubbed donor (D-) and acceptor (A-) are cast from solution mixtures to form thin films having nanosize domains of relatively pristine materials and large D-A interface area [128, 139, 140]. This type of BHJ structure usually allows for light absorption in the bulk donor domains that generate excitons, followed by exciton dissociation at the D-A interfaces. However the process by which the excitons reach the D-A interfaces and dissociate to generate separate charge polarons in the D-A nano-domains is only now being the focus of attention [27, 141].

It was originally postulated that once the exciton in the bulk donor domain reaches the D-A interface, it undergoes an ultrafast electron transfer to the acceptor forming a hole-polaron (P^+) in the donor and electron-polaron (P^-) in the acceptor, which are free to participate in the subsequent charge transport process towards the device electrodes [142]. However the mutual P^+-P^- Coulomb attraction should prevent a complete charge separation even if the offset energy of the donor and acceptor active levels is taken into account [75]. On the contrary, the bound P^+-P^- pair forms a charge transfer (CT) state at the D-A interface deep below the D and A optical gaps. However in spite of ample spectroscopic evidence for the existence of such CT state at the D-A interfaces [26, 75, 77, 79, 86, 143], it has been argued that it lies too deep in the gap to have any effect on the charge photogeneration process in the blends [98]. In this part we tried to elucidate the early stages of the charge photogeneration process in the prototype D-A blend, RR-P3HT and PCBM.

The P3HT polymers and PCBM fullerene were supplied by *Plextronics Inc.* [86]. The mixing ratio of the P3HT/PCBM blends was 1.2: 1 by weight, which gives the optimal PCE-value in solar cells [141]. The films were spin cast onto CaF_2 or CsI that are transparent in the mid-IR spectral range. The RR-P3HT/PCBM blend film was thermally annealed at 150 °C for 30 min to enhance the D-A domains size [141]; whereas the region-random RRa-P3HT/PCBM film was used as deposited.

1.3.1 Transient Photomodulation Spectroscopy of Pristine RR-P3HT Films

We measured $\Delta T(t)/T$ spectra of *pristine* polymer and fullerene films (Fig. 1.9). $\Delta T(0)/T$ spectrum of pristine RR-P3HT film (Fig. 1.9a) is dominated by a single PA_1

band at 1 eV followed by photo-bleaching above 1.97 eV and a small stimulated emission band at 1.75 eV, which attests to the excellent quality of the RR-P3HT polymer used here [86]. These three spectral features originate from photogenerated excitons since they decay together (Fig. 1.1a right inset) with an exponential time constant, $\tau_0 = 70$ ps. No photogenerated polarons which peak at 0.1 and 1.8 eV [see Fig. 1.11a inset] are observed here. Figure 1.9b shows $\Delta T(0)/T$ spectrum of pristine PCBM film. It is dominated by two PA bands, namely EX_1 and EX_2 at 1.0 and 2.25 eV, respectively that are due to photogenerated excitons. A third PA band, CT at 1.75 eV originates from charge-transfer excitons in the fullerene film, since it does not exist in the photomodulation spectrum of isolated PCBM molecules in polystyrene (Fig. 1.9b right inset). No photogenerated polarons which peak at 1.15 eV [129, 144] are discerned.

1.3.2 Photomodulation of RR-P3HT/PCMB Blends

1.3.2.1 Transient Photomodulation Spectroscopy with Above-Gap and Below-Gap Pump Excitations

To better understand the transient PA spectra in the polymer/fullerene blends we measured the x-ray diffraction (XRD) pattern from the RRa- and RR-P3HT/PCBM blend films (Fig. 1.10) using the Cu$K_{\square}$ X-ray line at $\lambda = 0.154$ nm. The XRD pattern of RR-P3HT/PCBM contains a prominent Bragg band at $2\theta_{[100]} = 5.3^{o}$ and its harmonics at $2\theta = 10.7^{o}$ and 16^{o}, respectively that originate from the P3HT nanocrystalline domains in the film [72]; as well as a smaller Bragg band at $2\theta_{[311]} = 19.3^{o}$ that originates from the PCBM nanocrystalline domains in the blend

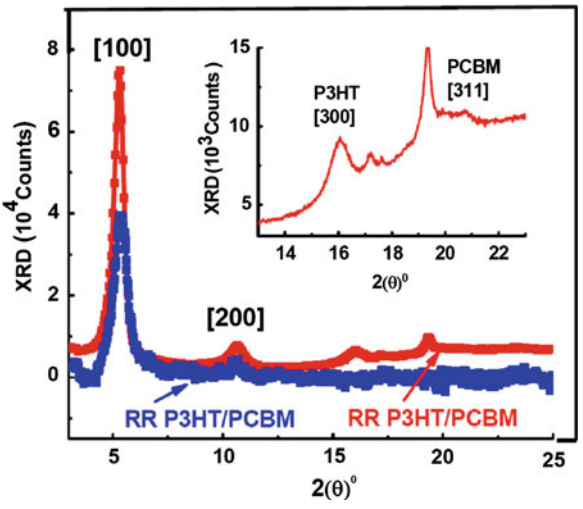

Fig. 1.10 The XRD pattern from RR-P3HT/PCBM (*red*) and RRa-P3HT/PCBM (*blue*), where the P3HT bands [100], [200] and [300] and PCBM band [311] are assigned; the inset focuses on the PCBM band (Adapted from Singh et al. [92])

[146]. We therefore conclude that the annealed RR-P3HT/PCBM blend film contains separate donor and acceptor crystalline domains. We may estimate the average nanocrystalline domain size, D from the full width at half maximum [FWHM], $\Delta_{2\theta}$ of the respective Bragg bands using the Scherrer relation: $D = 0.9\lambda/\Delta_{2\theta}\cos\theta$; we obtain $D \approx 16$ nm (20 nm) for the polymer (PCBM) nano-domains. In contrast, the XRD pattern of the RRa-P3HT/PCBM blend does not show prominent P3HT band harmonics, and in addition the PCBM band is missing (Fig. 1.10). These indicate that the PCBM molecules do not form well-separated domains here; instead, they penetrate into the P3HT lamellae and consequently are much closer on average to the polymer chains.

Figure 1.11a shows $\Delta T(t)/T$ spectra of RR-P3HT/PCBM blend. $\Delta T(0)/T$ spectrum is very similar to that of pristine RR-P3HT (Fig. 1.9a), indicating that excitons are initially photogenerated within the polymer domains. At $t > 0$ the excitons decay; however *no polarons are generated* at the expense of the exciton decay up to 300 ps since there is no PA build-up at low $\hbar\omega$(probe), where the polaron P_1 band dominates the absorption spectrum (as seen in Fig. 1.11a inset). We thus conclude that the photogenerated excitons in the polymer domains decay into a *new state* that is not separated free polarons. This new state must be related with the D-A interfaces in the films since the excitons do not form such a state in the pristine polymer, and we thus propose that is a CT exciton at the D-A interface. In contrast, the background PA spectrum in the mid-IR (Fig. 1.11a) is very similar to the P_1 band in the polaron doping induced absorption spectrum (Fig. 1.11a inset), showing that charge polarons are indeed photogenerated in this RR-P3HT/PCBM film but at later time; in agreement with the high solar cells efficiency based on this blend [86]. We thus conclude that the charge photogeneration process in the blend proceeds in two stages [27, 147]. The first stage is exciton trapping in CT states at the D-A interfaces, followed by a much slower CT state dissociation into free polarons in the D and A domains at $t \gg 2$ ns (=the time limit of our translation stage).

The exciton decay dynamics in the blend is much faster than in the pristine polymer (see PA_1 decays in Figs. 1.11a and 1.9a). The shorter lifetime in the blend is related to the exciton dynamics towards the D-A interfaces, and therefore we studied the PA_1 decay kinetics in more detail. PA_1 decay cannot be fit with a single or few exponential decay functions; nor can it be fit using a diffusion model [$\sim (1 + t/\tau)^{-1}$]. Alternatively, PA_1 decay can be fit using multiple power-law decays that originate from a Förester resonant energy transfer (FRET) into the CT exciton [148], averaged over the exciton initial distance from the D-A interface (see [92]). This model yields the following time dependent surviving exciton density N(t) in the polymer nano-grains;

$$N(t)/N(0) = \exp(-t/\tau_0)\left[m_1 + m_2\left(C_1 t^{1/2} - C_2 t^{1/3} + C_3 t^{1/6}\right)\right] \tag{1.3}$$

where $\tau_0 = 70$ ps is the natural exciton lifetime in RR-P3HT that is obtained from the PA_1 dynamics of Fig. 1.9; m_1 and m_2 are fitting parameters; and the C constants are given by the relations: $C_1 = 0.2u^{-3}$, $C_2 = 0.66u^{-2}$ and $C_3 = 0.54/u$, where

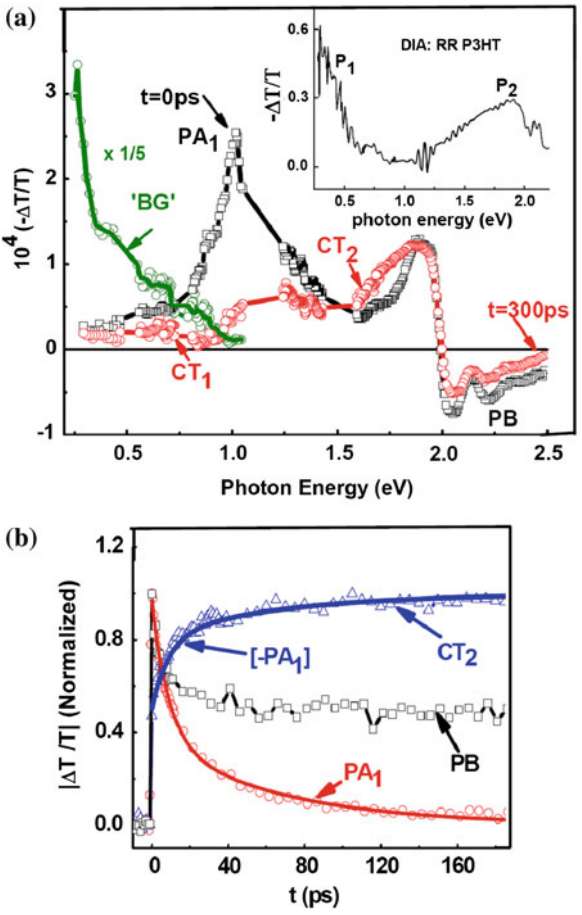

Fig. 1.11 **a** The transient photomodulation spectrum of RR-P3HT/PCBM blend film at t = 0 and t = 300 ps, respectively; the exciton band PA_1, and CT exciton bands CT_1 and CT_2 are indicated. The *green circles* and line represent the background (BG) PA spectrum measured at t = −5 ps. The *inset* shows the doping induced absorption of pristine RR-P3HT film, where the polaron bands P_1 and P_2 are assigned. **b** The transient decay of PA_1, build-up dynamics of CT_2, and the PB decay up to 180 ps. The line through the data points is a fit using the FRET mechanism (see text); the same function also fits the CT_2 build-up dynamics (Adapted from Singh et al. [92])

u = $D/2R_0$ is the parameter ratio of the grain size, D to twice the FRET radius, R_0, which was measured before to be between 3 and 9 nm [149]. Using R_0 = 6 nm and D = 16 nm from the XRD studies, we obtain u = 1.3. Subsequently the excellent fit to the PA_1 decay seen in Fig. 1.11b was obtained using $m_1 = 0.14$ and $m_2 = 7$.

In support of the CT intermediate role in the charge photogeneration process in the blend, Fig. 1.11a also shows that PA build-up indeed occurs in both mid-IR and near-IR [21] spectral ranges. In fact there are two PA bands, namely CT_1 in the mid-IR and CT_2 in the near-IR that are generated at longer time *at the expense of the exciton PA_1 decay*. Figure 1.11b shows that the CT_2 build-up dynamics in the near-IR closely matches the exciton PA_1 decay, since the same function of time fits both PA_1 decay and CT_2 build-up dynamics (measured at 1.75 eV probe). Figure 1.12a more clearly shows the two PA bands that are generated at the expense of the exciton PA_1 decay. To obtain the full photogenerated CT spectrum we subtracted the photomodulation spectrum at t = 30 ps from that at t = 0, after normalizing the two

PA bands at 1 eV and 2 eV for the CT_1 and CT_2 bands, respectively. It is seen that the CT spectrum contains two prominent PA bands that peak at 0.6 (CT_1) and 1.75 eV (CT_2), respectively, which are very different than the bands P_1 and P_2 of polarons (Fig. 1.11a inset). Consequently we propose that these two PA bands are due to optical transitions within the CT manifold at the D-A interfaces [27, 142].

To support this assumption we measured the transient photomodulation spectrum using $\hbar\omega$(pump) = 1.55 eV, which is below the optical gap of the polymer and fullerene constituents. Such low $\hbar\omega$(pump) can resonantly excite the CT state at the D-A interface since its energy was measured to be between 1.2 and 1.6 eV [86], without first photogeneration of excitons in the polymer domains. Figure 1.12b shows that under these conditions the two CT PA bands are instantaneously photogenerated; which is compelling evidence that they originate from the CT states at the interfaces. This supports our assignment for the CT bands in the transient photomodulation spectrum of this blend.

Interestingly the background PA spectrum excited with below-gap pump excitation (Fig. 1.12b) is very similar to that generated using above-gap pump excitation

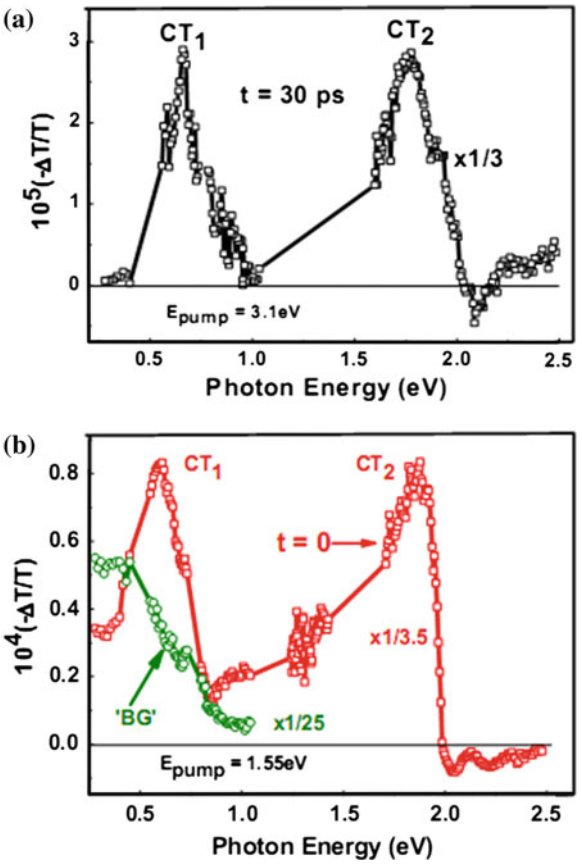

Fig. 1.12 **a** The transient photomodulation spectrum of RR-P3HT/PCBM blend film at t = 30 ps excited at 3.1 eV, normalized and subtracted from the spectrum at t = 0, that shows the two newly formed CT_1 and CT_2 bands. **b** Same as in **a** but at t = 0 and excited at 1.55 eV, which is below the gap of both polymer and fullerene constituents (Adapted from Singh et al. [92])

(Fig. 1.11a), which we identified as due to long-lived charge polarons [86]. This shows that there exists a mechanism where thermalized CT excitons at the D-A interfaces are able to separate into free polarons in the donor and acceptor domains, *regardless of the initial* $\hbar\omega$(pump) [27]. This finding is very important, since it can refute the notion that the CT state in the blend lies too deep in the gap to have any influence over the charge photogeneration process. Apparently the exciton kinetic energy when reaching the CT state plays a minor role in the charge photogeneration process; this may explain the flat spectral response of the photocurrent action spectrum in organic solar cells [86].

1.3.2.2 CW Photomodulation Spectroscopy with Above-Gap and Below-Gap Excitations

A compelling signature of photogenerated charges in π-conjugated polymers is the appearance of in-gap polaron PA bands, as seen in the PM spectrum of the blend shown in Fig. 1.13. We clearly identify the well-known polaron PA bands P_1 and P_2. In addition to the in-gap transitions, the polaron excitation also renormalizes the frequencies of the Raman active amplitude modes in the polymer chain, where the small polaron mass causes the IR active vibrations (IRAV) to possess very large oscillator strengths [96]. The below-gap pump excitation of the blend also produces the same polaron PA features as those produced with above-gap pump excitation; this confirms that polaron photogeneration is also possible with below-gap pump, in agreement with the transient PM data discussed above. We emphasize that the

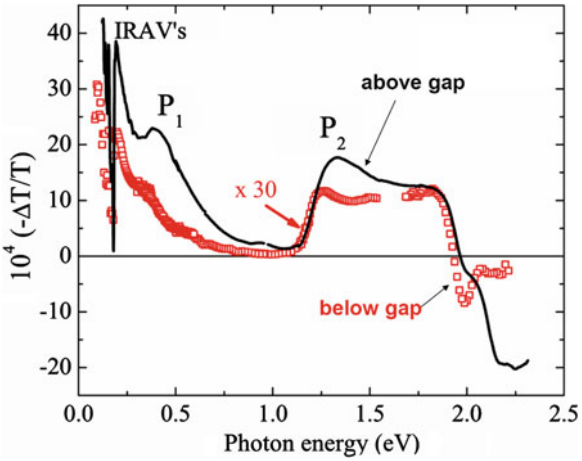

Fig. 1.13 CW PA spectra of RR-P3HT/PCBM film using above gap (*black solid line*) and below-gap (*red squares*) pump excitation. The AG (BG) pump excitation is at 2.5 (1.55) eV. Both spectra show the known PA band signature of polarons; namely, P_1, P_2 bands and IRAV, as denoted (Adapted from Drori et al. [86])

mechanism by which the polaron species are photogenerated with below-gap excitation cannot be explained by the known single-step photoinduced charge transfer reaction [21, 150]; since singlet excitons that supposedly precede charge dissociation are not photogenerated in the polymer or fullerene domains, as revealed in the picosecond transient PM spectrum (Fig. 1.11) [151].

To further investigate the process by which polarons are photogenerated with below-gap excitation we studied the polarons recombination dynamics generated with below-gap and above-gap pump excitations. The recombination dynamics was obtained from the modulation-frequency response of the P_1 band of the polarons using the bimolecular dispersive recombination model [113]. Figure 1.14 shows the PA response at temperature T = 30 K, and the fit using 1.2 from which the lifetime, τ, was obtained. We realize that τ dramatically increases with below-gap excitation.

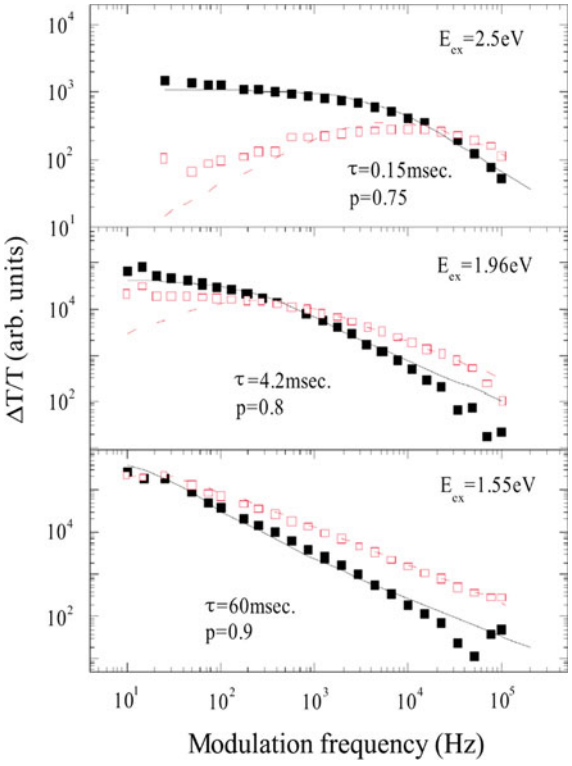

Fig. 1.14 Modulation frequency dependence of the P_1 PA polaron band in RR-P3HT/PCBM blend measured at 0.4 eV and T = 30 K; both in-phase (*full black squares*) and quadrature (*empty red squares*) PA are shown. The *lines* through the data points are fit using 1.2 where the best-fit lifetime, τ and dispersive parameter exponent, p are indicated. The various panels represent different pump excitation: *top panel* is for above-gap excitation pumped at 2.5 eV; *middle panel* is for below-gap excitation pump at 1.96 eV; *bottom panel* is for below-gap excitation at 1.55 eV (Adapted from Drori et al. [86])

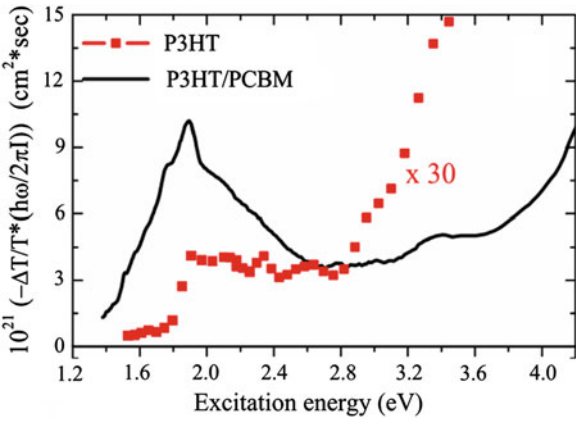

Fig. 1.15 Pump excitation dependence of polarons RR-P3HT/PCBM blend measured at T = 30 K. Polaron band P_1 action spectra for RR-P3HT (*squares*) and RR-P3HT/PCBM blend (*solid line*) measured between 0.25 and 0.4 eV, normalized to the impinging excitation photon flux (Adapted from Drori et al. [86])

The increase in τ is by about three orders of magnitude, from τ = 150 μs with above-gap pump excitation at $\hbar\omega$ = 2.5 eV to τ = 60 ms with below-gap excitation at $\hbar\omega$ = 1.55 eV. This shows that below-gap photogenerated polarons have much slower recombination kinetics. For the diffusion-limited bimolecular kinetics known to exist in polymers [113], this indicates either increased localization for the below-gap photogenerated polarons or charge separation into two different phases, namely, the polymer and fullerene domains.

We also used the polaron action spectrum for understanding the below-gap polaron photogeneration process, where we probe the strength of the polaron P_1 band between 0.25 and 0.4 eV as a function of the excitation $\hbar\omega$, normalizing by the impinging excitation photon flux, I. Figure 1.15 shows the polaron action spectra for pristine P3HT and P3HT/PCBM blend. The polaron photogeneration action spectrum of pristine P3HT has a clear onset at the polymer band edge $\hbar\omega$ = 1.85 eV; and lacks the below-gap polaron generation component. In contrast, the polaron photogeneration action spectrum in the blend extends to $\hbar\omega$ pump well into the polymer optical gap with an extrapolated onset at $\hbar\omega$ = 1.2 eV, i.e., much smaller than the polymer and fullerene absorption edges. In addition the polaron action spectrum also shows a prominent peak at ∼1.9 eV having an apparently smaller polaron generation efficiency for $\hbar\omega$ > Eg (the polymer optical gap). This (as well as Fig. 1.6b) is an illusion, however, since the polaron lifetime is longer with below-gap excitation. This so called "lifetime effect" dramatically influences the polaron action spectrum, since the measurements are done at steady-state conditions, where the polaron density is also influenced by their recombination lifetime [26, 86]. Nevertheless, this effect in the polaron action spectrum can be corrected by considering the lifetime difference measured at different pump excitations [86].

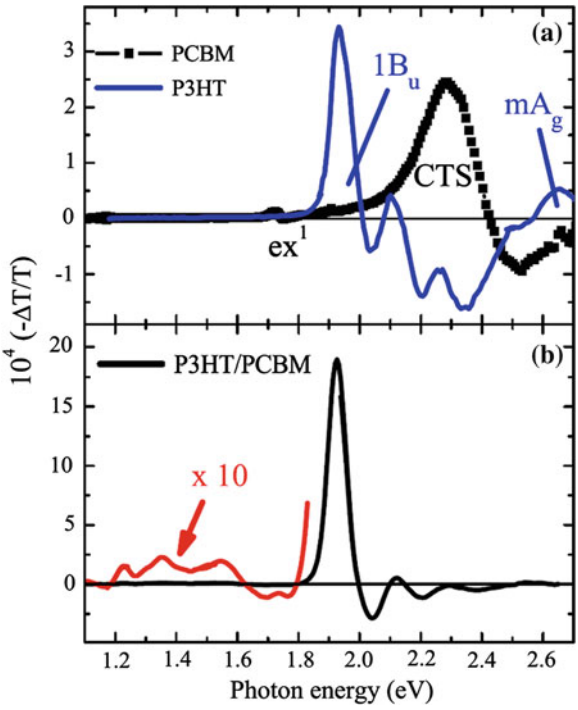

Fig. 1.16 **a** The EA spectra of pristine RR-P3HT (*blue line*) and PCBM (*black squares*). $1B_u$ and mA_g denote strongly coupled exciton states in the polymer; whereas CTS denotes the charge transfer state in the fullerene. **b** The EA spectrum of RR-P3HT/PCBM blend, where the below-gap spectrum is also shown multiplied by a factor of 10. The CTC in the blend is denoted (From Drori et al. [86] with Permission)

1.3.2.3 Electroabsorption Spectroscopy

The mechanism by which below-gap polaron photogeneration occurs without involving exciton formation may be better understood by involving a CTC state at the interface between the polymer and fullerene domains, that lies below the optical gap of the blend material constituents. One viable way to measure such a CTC state is using the EA spectroscopy; since such a state may have a large dipole moment that enhances the EA signal [83–85].

The EA spectrum of the pristine RR-P3HT (Fig. 1.16a) is dominated by the strongly coupled exciton transitions $1B_u$ and mA_g at 2.0 eV and 2.7 eV, respectively [73]. Whereas the EA spectrum of PCBM reveals the charge transfer state (denoted CTS) transition at 2.4 eV [26] in this material. We note that there are no optical EA features below the polymer and fullerene optical gaps for the pristine polymer and fullerene films. In contrast, an EA band with an onset at 1.2 eV is obtained in the blend (Fig. 1.16b). A broad derivative-like feature can be seen, followed by a broad-band that spans $\hbar\omega$(probe) range from 1.2 to 1.8 eV with several clear peaks. We assign this new EA feature to the CTC state in the gap and speculate that the various secondary peaks are due to excited states in the CTC manifold. We note that although the CTC states are mainly formed at the polymer/fullerene interfaces with relatively small cross section, it is still possible to observe its associated optical transitions using EA spectroscopy due to its strong coupled dipole moment [83, 84];

this can be barely achieved using linear absorption measurements [114]. The EA onset at 1.2 eV, which we interpret here as the onset of the CTC manifold, is the lowest $\hbar\omega$ obtained for the CTC so far in any blend. [75, 81] This may be an important contributing factor for the high PCE of ~4.2 % obtained for the OPV device based on the RR-P3HT/PCBM blend.

1.3.3 Photomodulation of Pristine RRa-P3HT and RRa-P3HT/PCMB Blends; a Comparison

For comparison, we also study the charge photogeneration mechanism in RRa-P3HT/PCBM blend where the fullerene molecules are closer to the polymer chains on average. Figure 1.17a shows $\Delta T(t)/T$ spectra of *pristine* RRa-P3HT. It also contains a single PA_1 exciton band at ~1 eV followed by stimulated emission above ~1.75 eV that shares the same dynamics (Fig. 1.17a inset). However $\Delta T(0)/T$ spectrum in RRa-P3HT/PCBM blend (Fig. 1.18a) is very different from that in RR-P3HT/PCBM blend (Fig. 1.11a). The former spectrum shows the same two CT PA bands (namely CT_1 and CT_2 discussed above) that are generated within ~500 fs (Fig. 1.18b), in concert with the ultrafast decay of the exciton PA_1 band. The fast exciton decay here is consistent with the proximity of the PCBM molecules to the P3HT polymer chains in RRa-P3HT/PCBM blend. Interestingly,

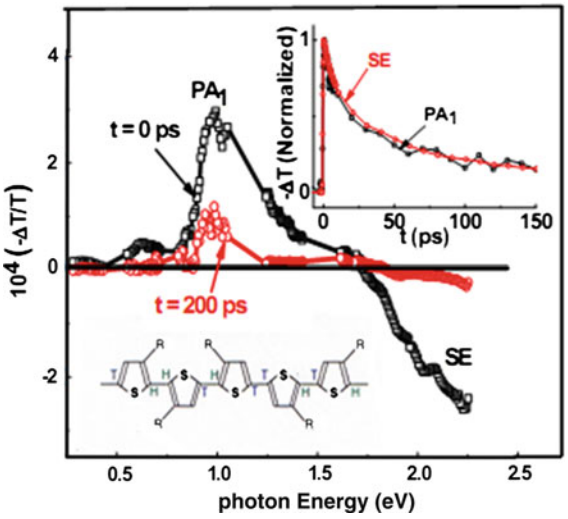

Fig. 1.17 The transient photomodulation spectrum of pristine RRa-P3HT film at t = 0 and t = 200 ps, respectively; the exciton bands PA_1 and SE are indicated. The *right inset* shows the transient decay of PA_1 and SE bands up to t = 200 ps; the *left inset* shows the polymer backbone chain (Adapted from Singh et al. [92])

the background PA spectrum here does not show long-lived polaron photogeneration; in fact the background PA spectrum is the *same* as the transient PA spectrum. This shows that the photogenerated CT excitons in this blend cannot easily dissociate into free polarons, in agreement with the poor solar cell efficiency (<0.1 %) based on this blend (Fig. 1.19). It also shows that the CT exciton dissociation is related to the D-A domain size. The larger is the D-A interface area the smaller is the CT exciton binding energy, and consequently the more efficient is the CT exciton dissociation into separate charge polarons in the D and A domains [88].

This conclusion is further supported by the I-V characteristics under solar-like illumination of photovoltaic devices based on RR-P3HT/PCBM and RRa-P3HT/PCBM blends using AM1.5 filter as shown in Fig. 1.19. It is seen that the power conversion efficiency and short circuit current of RR-P3HT/PCBM blend are more than an order of magnitude higher than that of RRa-P3HT/PCBM blend.

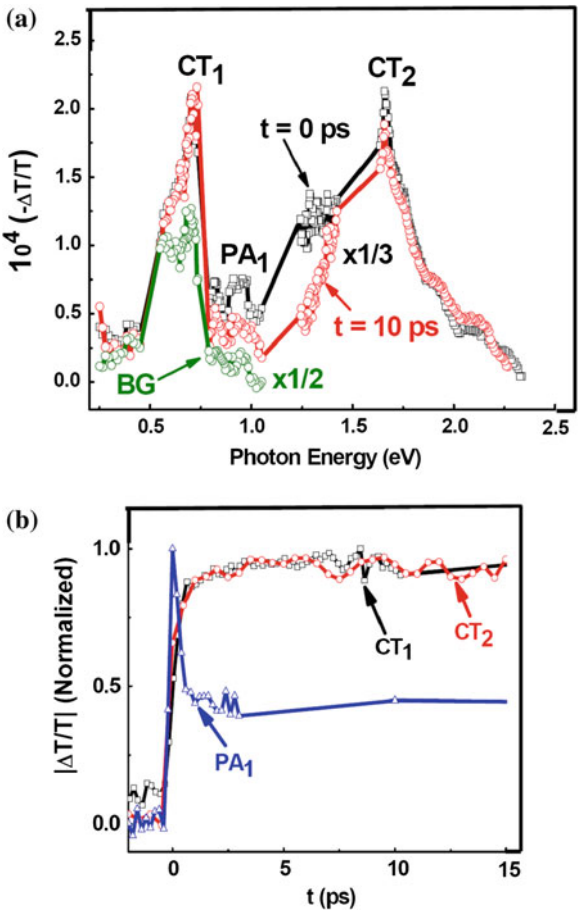

Fig. 1.18 **a** The transient photomodulation spectrum of RRa-P3HT/PCBM blend at t = 0 and t = 10 ps, respectively excited at 3.1 eV; the PA bands PA_1, CT_1 and CT_2 are assigned. **b** The transient decay of PA_1, and build-up dynamics of CT_1 and CT_2 up to 15 ps (Adapted from Singh et al. [92])

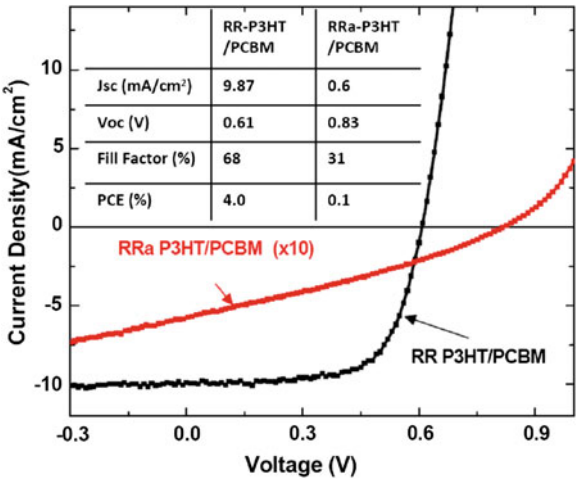

Fig. 1.19 The I-V characteristic of two solar cells based on PCBM blend with RR-P3HT (*black*) and RRa-P3HT (*red*) donor polymers under solar-like illumination of AM 1.5. The inserted Table gives the device photovoltaic characteristic parameters such as short circuit current density, J_{sc}; open-circuit voltage, V_{oc}; fill-factor, FF; and the power conversion efficiency, PCE in % (From Singh et al. [92] with permission)

1.4 Summary

In this chapter, we reviewed the studies of photophysics in two typical π-conjugated polymers, namely RR-P3HT with self-organized π-stacked two-dimensional lamellae and MEH-PPV with amorphous nanomorphology in pristine and blend with fullerene molecules, using a variety of optical probe techniques including broadband femtosecond transient and continuous wave (cw) photomodulation spectroscopies and electroabsorption. In polymer/fullerene blends the photogenerated excitons quickly decay away to give rise to a novel photoexcitation. We provide strong evidence for the existence of charge transfer complex (CTC) state (charge transfer excitons) that is formed inside the optical gap of the polymer and fullerene constituents, which is clearly revealed in the electro-absorption spectrum. Because of the below-gap CTC it is possible to directly generate polarons in the blends without involving intrachain excitons in the polymer phase, with below gap pump excitation. The CTC state lying inside the gap readily explains both the below-gap excitation and near-IR photoluminescence in the blend. Moreover, using action spectra of polaron PA we showed that the polaron generated with below-gap excitation are more localized compared with polarons with above-gap excitation.

In RR-P3HT/PCBM blend with typical D-A bulk heterojunction morphology we demonstrated that the charge photogeneration mechanism in organic solar cells occurs in two-steps. First the photogenerated excitons in the polymer domains reach the D-A interfaces within few *ps* time depending on the domain size, where they

form CT excitons. This process is followed by CT exciton dissociation into free charged polarons in the D and A domains in the *ns–μs* time scale, which remains to be observed. The CT exciton dissociation depends on the CT exciton binding energy, which is significantly lower for larger D-A interface area. Our results emphasize the importance of the D-A domain size in organic solar cells based on bulk heterojunction morphology.

In MEH-PPV/C_{60} blend (1:1 by weight) as well as in RRa-P3HT/PCBM blend, the low degree of phase separation in the blend results in the fast dissociation (<200 fs) of excitons generated in the polymer chains (as well as results in the fast populating of CTC states on the interface). However, the polarons generated from further dissociation of CTC are localized because of amorphous morphology of MEH-PPV and RRa-P3HT film.

Our findings indicate that the CTC state and film morphology play a crucial role in carrier photogeneration in donor-acceptor blends. More thorough exploration of the CT excitation their interaction with free polaron excitations may improve the power conversion efficiency of organic solar cell and drive the development of novel photoactive materials.

Acknowledgments We would like to thank our collaborators at the University of Utah Physics Department over the years 2000–2012, without whom this work would have never been completed. These are T. Basel, T. Drori, J. Holt, E. Olejnik, B. Pandit, R.C. Polson, S. Singh, M. Tong, C. Yang, and C. Wu. We also acknowledge useful collaboration with S. Mazumdar from the University of Arizona, E. Ehrenfreund from the Technion in Israel, and S. Li and D. Laird from Plextronics.

This work was supported in part over the years by the Department of Energy grant No. FG-04-ER46109. C.-X. Sheng thanks the support of NSF of China No. 61006014, NHTRDP of China, No. 2011AA050520, the Fundamental Research Funds for the Central Universities No. 3092013-0111008.

References

1. L. Dou, J. You, J. Yang, et al., Nature Photonics **6**, 180 (2012)
2. M.A. Green, K. Emery, Y. Hishikawa, W. Warta, Prog. Photovoltaics **19**, 84 (2011)
3. M.A. Green, K. Emery, Y. Hishikawa et al., Prog. Photovoltaics **20**, 12 (2012)
4. T.M. Clarke, J.R. Durrant, Chem. Rev. **110**, 6736 (2010)
5. C. Deibel, T. Strobel, V. Dyakonov, Adv. Mater. **22**, 4097 (2010)
6. Primary Photoexcitations in Conjugated Polymers: Molecular Exciton versus Semiconductor Band Model (ed.) by S. Sariciftci (World Scientific, Singapore, 1997)
7. M. Tong et al., Phys. Rev. B **75**, 125207 (2007)
8. M. Chandross, S. Mazumdar, S. Jeglinski, X. Wei, Z.V. Vardeny, E.W. Kwock, T.M. Miller, Phys. Rev. B **50**, 14702 (1994)
9. H. Zhao, S. Mazumdar, C.-X. Sheng, M. Tong, Z.V. Vardeny, Phys. Rev. B **73**, 075403 (2006)
10. Z.V. Vardeny, et al., Phys. Rev. Lett. **51**, 2326 (1983)
11. B. Horovitz, H. Gutfreund, M. Weger, Phys. Rev. B **17**, 2796 (1978)
12. E. Ehrenfreund et al., Phys. Rev. B **36**, 1535 (1987)
13. N.S. Sariciftci, L. Smilowitz, A.J. Heeger, F. Wudl, Science **258**, 1474 (1992)

14. G. Yu, J. Ga, J.C. Hummelen et al., Science **270**, 1789 (1995)
15. P. Shaw, A. Ruseckas, I. Samuel, Adv. Mater. **20**, 3516 (2008)
16. A. Huijser, T.J. Savenije, A. Shalav, L.D. Siebelles, J. Appl. Phys. **104**, 034505 (2008)
17. J.E. Kroeze, T.J. Savanije, M.J.W. Vermeulen, J.M. Warman, J. Phys. Chem. B **107**, 7696 (2003)
18. A. Haugeneder, M. Neges, C. Kallinger et al., Phys. Rev. B **59**, 15346 (1999)
19. W. Ma, C. Yang, X. Gong, K. Lee, A.J. Heeger, Adv. Funct. Mater. **15**, 1617 (2005)
20. N. Banerji, S. Cowan, E. Vauthey, A.J. Heeger, J. Phys. Chem. C **115**, 9726 (2011)
21. W. Hwang, D. Moses, A.J. Heeger, J. Phys. Chem. C **112**, 4350 (2008)
22. I.A. Howard, R. Mauer, M. Meister, F. Laquai, J. Am. Chem. Soc. **132**, 14866 (2010)
23. A.L. Ayzner, C.J. Tassone, S.H. Tolbert, B.J. Schwartz, J. Phys. Chem. C **113**, 20050 (2009)
24. J.-L. Brédas, J.E. Norton, J. Cornil, V. Coropceanu, Acc. Chem. Res. **42**, 1691 (2009)
25. T. Strobel, C. Deibel, V. Dyakonov, Phys. Rev. Lett. **105**, 266602 (2010)
26. T. Drori, C.X. Sheng, A. Ndobe et al., Phys. Rev. Lett. **101**, 037401 (2008)
27. A.A. Bakulin, A. Rao, V.G. Pavelyev et al., Science **335**, 1340 (2012)
28. X. Wei et al., Phys. Rev. Lett. **68**, 666 (1992)
29. M. Tong et al., Phys. Rev. B **75**, 125207 (2007)
30. C.-X. Sheng, M. Tong, S. Singh, Z.V. Vardeny, Phys. Rev. B **75**, 085206 (2007)
31. Z. V. Vardeny, X. Wei., in *Handbook of Conducting Polymers*, edited by T.A. Skotheim, R. L. Elsenbaumer, J. Reynolds (2nd Ed.), (Marcel Dekker Inc., New York, 1998)
32. K. Fesser et al., Phys. Rev. B **27**, 4804 (1983)
33. Z.V. Vardeny, J. Tauc, Phys. Rev. Lett. **54**, 1844 (1985)
34. Z.G. Soos, S. Ramasesha, Phys. Rev. B **29**, 5410 (1984)
35. S.V. Frolov et al., Phys. Rev. B **65**, 205209 (2002)
36. A.J. Heeger et al., Rev. Mod. Phys. **60**, 781 (1988)
37. S.N. Dixit, D. Guo, S. Mazumdar, Phys. Rev. B **43**, 6781 (1991)
38. D. Guo et al., Phys. Rev. B **48**, 1433 (1993)
39. F. Paquin, G. Latini, M. Sakowicz et al., Phys. Rev. Lett. **106**, 197401 (2011)
40. P.B. Miranda, D. Moses, A.J. Heeger, Phys. Rev. B **64**, 081201 (2001)
41. K. Aryanpour, C.-X. Sheng, E. Olejnik, B. Pandit, D. Psiachos, S. Mazumdar, Z.V. Vardeny, Phys. Rev. B **83**, 155124 (2011)
42. R. Kersting et al., Phys. Rev. Lett. **73**, 1440 (1994)
43. J.B. Birks, *Photophysics of Aromatic Molecules* (Wiley, London, 1970)
44. N.T. Harison et al., Phys. Rev. Lett. **77**, 188 (1996)
45. M. Pope, C.E. Swenberg, *Electronic Processes in Organic Crystals and Polymers*, 2nd edn. (Oxford University Press, Oxford, 1999)
46. M.W.B. Wilson, A. Rao, J. Clark, R.S.S. Kumar, D. Brida, G. Cerullo, R.H. Friend, J. Am. Chem. Soc. **133**, 11830 (2011)
47. P.M. Zimmerman, Z. Zhang, C.B. Musgrave, Nat. Chem. **2**, 648 (2010)
48. P. Miranda, D. Moses, A.J. Heeger, Phys. Rev. B **70**, 085212 (2004)
49. C. Gadermaier, G. Cerullo, G. Sansone, G. Leising, U. Scherf, G. Lanzani, Phys. Rev. Lett. **89**, 117402 (2002)
50. Rothberg, L., in *Semiconducting Polymers: Chemistry, Physics and Engineering,* vol. I, edited by G. Hadziioannou, G. G. Malliaras (Wiley, New York, 2006), pp. 179–204 (and references therein)
51. V.I. Arkhipov, H. Bässler, Phys. Status Solidi A **201**, 1152 (2004). (and references therein)
52. B.J. Schwartz, Annu. Rev. Phys. Chem. **54**, 141 (2003). and references therein
53. Conwell, E.M. in *Organic Electronic Materials: Conjugated Polymers and Low Molecular Weight Solids*, edited by R. Farchioni, G. Grosso (Springer, New York, 2001), pp. 127–180
54. I.D.W. Samuel, G. Rumbles, C.J. Collison, Phys. Rev. B **52**, R11573 (1995)
55. I.D.W. Samuel, G. Rumbles, C.J. Collison, S.C. Moratti, A.B. Holmes, Chem. Phys. **227**, 75 (1998)
56. P.K.H. Ho, J.-S. Kim, N. Tessler, R.H. Friend, J. Chem. Phys. **115**, 2709 (2001)
57. S.-H. Lim, T.G. Bjorklund, K.M. Gaab, C.J. Bardeen, J. Chem. Phys. **117**, 454 (2002)

58. P.J. Brown, D.S. Thomas, A. Köhler et al., Phys. Rev. B **67**, 064203 (2003)
59. A.B. Koren, M.D. Curtis, A.H. Francis, J.W. Kampf, J. Am. Chem. Soc. **125**, 5040 (2003)
60. J. Clark, C. Silva, R.H. Friend, F.C. Spano, Phys. Rev. Lett. **98**, 206406 (2007)
61. S. Singh, T. Drori, Z.V. Vardeny, Phys. Rev. B **77**, 195304 (2008)
62. B. Schweitzer, V.I. Arkhipov, H. Bässler, Chem. Phys. Lett. **304**, 365 (1999)
63. D. Hertel, Y.V. Romanovskii, B. Schweitzer, U. Scherf, H. Bässler, Synth. Met. **116**, 139 (2001)
64. Y. Zhang, Z. Wang, M.-K. Ng, L.J. Rothberg, J. Phys. Chem. B **111**, 13211 (2007)
65. V. Morandi, M. Galli, F. Marabelli, D. Comoretto, Phys. Rev. B **79**, 045202 (2009)
66. M. Yan et al., Phys. Rev. Lett. **72**, 1104 (1994)
67. H.A. Mizes, E.M. Conwell, Phys. Rev. B **50**, 11243 (1994)
68. P.A. Lane, X. Wei, Z.V. Vardeny, Phys. Rev. B **56**, 4626 (1997)
69. D.K. Campbell et al., Phys. Rev. B **26**, 6862 (1982)
70. M. Wohlgenannt, X.M. Jiang, Z.V. Vardeny, Phys. Rev. B **69**, 241204 (2004)
71. Z.V. Vardeny et al., Phys. Rev. Lett. **56**, 671 (1986)
72. H. Sirringhaus et al., Nature **401**, 685 (1999)
73. R. Österbacka et al., Science **287**, 839 (2000)
74. X.M. Jiang et al., Adv. Funct. Mater. **12**, 587 (2002)
75. J.J. Benson-Smith, L. Goris, K. Vandewal et al., Adv. Funct. Mater. **17**, 451 (2007)
76. M.A. Loi, S. Toffanin, M. Muccini et al., Adv. Funct. Mater. **17**, 2111 (2007)
77. M. Hallermann, S. Haneder, E. Da Como, Appl. Phys. Lett. **93**, 053307 (2008)
78. P. Parkinson, J. Lloyd-Hughes, M.B. Johnston, L.M. Herz, Phys. Rev. B **78**, 115321 (2008)
79. A.A. Bakulin, S.A. Zapunidy, Pshenichnikov, et al., Phys. Chem. Chem. Phys. **11**, 7324 (2009)
80. J. Holt, S. Singh, T. Drori, Y. Zhang, Z.V. Vardeny, Phys. Rev. B **79**, 195210 (2009)
81. M. Hallermann, I. Kriegel, E. Da Como et al., Adv. Funct. Mater. **19**, 3662 (2009)
82. J.L. Brédas, D. Beljonne, V. Coropceanu, J. Cornil, Chem. Rev. **104**, 4971 (2004)
83. Z.D. Wang, S. Mazumdar, A. Shukla, Phys. Rev. B **78**, 235109 (2008)
84. K. Aryanpour, D. Psiachos, S. Mazumdar, Phys. Rev. B **81**, 085407 (2010)
85. H. Alves, A.S. Molinari, H.X. Xie, A.F. Morpurgo, Nat. Mater. **7**, 574 (2008)
86. T. Drori, J. Holt, Z.V. Vardeny, Phys. Rev. B **82**, 075207 (2010)
87. V. Dyakonov, E. Frankevich, Chem. Rev. **227**, 203 (1998)
88. V.I. Arkhipov, P. Heremans, H. Bassler, Appl. Phys. Lett. **82**, 4605 (2003)
89. S. Westenhoff et al., J. Am. Chem. Soc. **130**, 13653 (2008)
90. D. Veldman et al., J. Am. Chem. Soc. **130**, 7721 (2008)
91. A.C. Morteani et al., Phys. Rev. Lett. **92**, 247402 (2004)
92. S. Singh, B. Pandit, T.P. Basel, S. LI, D. Laird, Z.V. Vardeny, Phys. Rev. B **85**, 205206 (2012)
93. B. Horovitz, Solid State Commun. **41**, 729 (1982)
94. C.-X. Sheng, T. Basel, B. Pandit, Z.V. Vardeny, Org. Electron. **13**, 1031 (2012)
95. M.J. Rice, Phys. Rev. Lett. **37**, 36 (1976)
96. R. Österbacka, X.M. Jiang, C.P. An, B. Horovitz, Z.V. Vardeny, Phys. Rev. Lett. **88**, 226401 (2002)
97. V. Mizrahi et al., Synth. Metals **102**, 1182, 1999; *ibid* 119, 507 (2001)
98. J. Holt., Ph.D. thesis, University of Utah, 2009
99. O. Epshtein, G. Nakhmanovich, Y. Eichen, E. Ehrenfreund, Phys. Rev. B **63**, 125206 (2001)
100. R.K. Willardson, A.C. Beer eds , *Semiconductors and Semimetals,* vol. 9 (Academic Press, New York 1972)
101. L. Sebastian, G. Weiser, H. Bassler, Chem. Phys. **61**, 125 (1981)
102. G. Weiser, Phys. Rev. B **45**, 14076 (1992)
103. L. Sebastian, G. Weiser, Phys. Rev. Lett. **46**, 1156 (1981)
104. M. Liess, S. Jeglinski, Z.V. Vardeny et al., Phys. Rev. B **56**, 15712 (1997)
105. Ye. Zhang, Ph.D. Thesis, University of Utah, 2010

106. L. Rothberg., Proc. Int. School *of Physics "Enrico Fermi" Course CXLIX,* (eds.), V.M. Agranocich, G.C. La Rocca (IOS Press, Amsterdam, 2002), p. 299
107. E. Hendry et al., Phys. Rev B **71**, 125201 (2005)
108. C. Brabec et al., Chem. Phys. Lett. **340**, 232 (2001)
109. A. Kohler, D.A.D. Santos, D. Beljonne, et al.,Nature **392**, 903 (1998)
110. C.X. Sheng, Ph.D. Thesis, University of Utah, 2005
111. K. Yoshino et al., Jpn. J. Appl. Phys. Part 2, **32**, L140 (1993)
112. S.V. Frolov et al., Chem. Phys. Lett. **286**, 2 (1998)
113. O. Epshtein et al., Phys. Rev. Lett. **90**, 046804 (2003)
114. L. Goris et al., Appl. Phys. Lett. **88**, 052113 (2006)
115. P. Panda et al., J. Phys. Chem. B **111**, 5076 (2007)
116. C. Winder, N. Sariciftci, Mater. Chem. **14**, 1077 (2004)
117. N.H. Karam, R.R. King, M. Haddad et al., Sol. Energy Mater. Sol. Cells **66**, 453 (2001)
118. J.Y. Kim, K. Lee, N.E. Coates et al., Science **317**, 222 (2007)
119. A.A. Bakulin, S.G. Elizarov, A.N. Khodarev et al., Synth. Met. **147**, 221 (2004)
120. D.Y. Paraschuk, S.G. Elizarov, A.N. Khodarev et al., JETP Lett. **81**, 467 (2005)
121. C. Im, J.M. Lupton, P. Schouwink, S. Heun, H. Becker, H. Bässler, J. Chem. Phys. **117**, 1395 (2002)
122. J.E. Kuder, J.M. Pochan, S.R. Turner, D.F. Hinman, J. Electrochem. Soc. **125**, 1750 (1978)
123. J.G. Müller, J.M. Lupton, J. Feldmann et al., Phys. Rev. B **72**, 195208 (2005)
124. W.D. Gill, J. Appl. Phys. **43**, 5033 (1972)
125. A.A. Bakulin, D.S. Martyanov, D.Y. Paraschuk et al., J. Phys. Chem. B **112**, 13730 (2008)
126. G. Dennler, M.C. Scharber, C.J. Brabec, Adv. Mater. **21**, 1223 (2009)
127. G. Li, V. Shrotriya, J. Huang et al., Nat. Mater. **4**, 864 (2005)
128. R.A. Marsh, J.M. Hodgkiss, S. Albert-Seifried, R.H. Friend, Nano Lett. **10**, 923 (2010)
129. J. Guo, H. Ohkita, H. Benten, S. Ito, J. Am. Chem. Soc. **132**, 6154 (2010)
130. I. Montanari, A.F. Nogueira, J. Nelson et al., Appl. Phys. Lett. **81**, 3001 (2002)
131. A.J. Ferguson, N. Kopidakis, S.E. Shaheen, G. Rumbles, J. Phys. Chem. C **115**, 23134 (2011)
132. K. Kanemoto, M. Yasui, T. Higuchi et al., Phys. Rev. B **83**, 205203 (2011)
133. J. Clark, J.-F. Chang, F.C. Spano et al., Appl. Phys. Lett. **94**, 163306 (2009)
134. R. Österbacka, C.P. An, X.M. Jiang, Z.V. Vardeny, Synth. Met. **116**, 317 (2001)
135. J. Piris, T.E. Dykstra, A.A. Bakulin et al., J. Phys. Chem. C **113**, 14500 (2009)
136. D. Veldman, S.C.J. Meskers, R.A.J. Janssen, Adv. Funct. Mater. **19**, 1939 (2009)
137. J. Cabanillas-Gonzalez, G. Grancini, G. Lanzani, Adv. Mater. **23**, 5468 (2011)
138. M.R. Wasielewski, Chem. Rev. **92**, 435 (1992)
139. M. Campoy-Quiles, T. Ferenczi, T. Agostinelli et al., Nat. Mater. **7**, 158 (2008)
140. R.A. Marsh, J.M. Hodgkiss, S.A. Seifried, R.H. Friend, Nano Lett. **10**, 923 (2010)
141. G. Li, R. Zhu, Y. Yang, Nature Photon. **6**, 153 (2012)
142. X.Y. Zhu, Q. Yang, M. Muntwiler, Acc. Chem. Res. **42**, 1779 (2009)
143. J.W. Kiel, A.P.R. Eberle, M.E. Mackay, Phys. Rev. Lett. **105**, 168701 (2010)
144. S. Yamamoto, J. Guo, H. Ohkita, S. Ito, Adv. Funct. Mater. **18**, 2555 (2008)
145. H. Ohkita, S. Ito, Polymer **52**, 4397 (2011)
146. P.H. Heiney, J.E. Fischer, A.R. McGhie et al., Phys. Rev. Lett. **66**, 2911 (1991)
147. J. Lee, K. Vandewal, S.R. Yost et al., J. Am. Chem. Soc. **132**, 11878 (2010)
148. T. Forster, Discuss. Faraday Soc. **27**, 7 (1959)
149. D.C. Coffey, A.J. Ferguson, N. Kopidakis, G. Rumbles, ACS Nano **4**, 5437 (2010)
150. S. Morita, A.A. Zakhidov, K. Yoshino, Solid State Commun. **82**, 249 (1992)
151. R. Mondal, S. Ko, J.E. Norton et al., J. Mater. Chem. **19**, 7195 (2009)
152. L.J.A. Koster, V.D. Mihailetchi, P.W.M. Blom, Appl. Phys. Lett. **88**, 052104 (2006)

http://www.springer.com/978-3-662-45508-1

Progress in High-Efficient Solution Process Organic Photovoltaic Devices
Fundamentals, Materials, Devices and Fabrication
Yang, Y.; Li, G. (Eds.)
2015, XVII, 417 p. 216 illus., 63 illus. in color.,
Hardcover
ISBN: 978-3-662-45508-1